*minerals*

MDPI

*Article*

# Geochemistry of Hydrothermal Alteration Associated with Cenozoic Intrusion-Hosted Cu-Pb-Zn Mineralization at Tavşanlı Area, Kütahya, NW Turkey

**Mustafa Kumral [1,*], Amr Abdelnasser [1,2] and Murat Budakoglu [1]**

[1] Department of Geological Engineering, Faculty of Mines, Istanbul Technical University, Istanbul 34469, Turkey; amrkhalil@itu.edu.tr (A.A.); budak@itu.edu.tr (M.B.)

[2] Department of Geology, Faculty of Science, Benha University, Benha 13518, Egypt

* Correspondence: kumral@itu.edu.tr; Tel.: +90-212-285-6307

Academic Editor: Maria Economou-Eliopoulos

Received: 18 December 2015; Accepted: 6 February 2016; Published: 17 February 2016

**Abstract:** The Miocene magmatic intrusion in the Tavşanlı zone of the Kütahya-Bolkardağ Belt (KBB) in the northwestern region of Turkey is represented by the Eğrigöz granitoids. This paper studies the petrology and geochemistry of hydrothermal alterations associated with the vein-type Cu-Pb-Zn mineralization hosted by this pluton, focusing on the determination of the mass gains and losses of chemical components, which reflect the chemical exchanges between the host rocks and hydrothermal fluids. Vein-type Cu-Pb-Zn mineralization is closely associated with intense hydrothermal alterations within the brecciation, quartz stockwork veining, and brittle fracture zones that are controlled by NW-SE trending faults cutting through the Eğrigöz granitoids. Paragenetic relationships reveal three stages of mineralization: pre-ore, ore, and supergene. The ore mineralogy typically includes hypogene chalcopyrite, sphalerite, galena, and pyrite, with locally supergene covellite, malachite, and azurite. Wall-rock hypogene hydrothermal alterations include pervasive silicification, sulfidation, sericitization, and selective carbonatization and albitization. These are distributed in three main alteration zones (zone 1: silicified/iron carbonatized alterations ± albite, zone 2: argillic-silicic alterations, and zone 3: phyllic alterations). Based on the gains and losses of mass and volume (calculated by the GEOISO-Windows™ program), zone 1 has a higher mass and volume gain than zones 2 and 3. Non-systematic zonal distributions of alterations are observed in which the silicic-carbonate alterations +/− albitization appeared in zone 1 in the center and the phyllic-argillic alterations appeared in zones 2 and 3, with an increase in base metals (Cu-Pb-Zn) in the zone from Cu, Cu-Pb, to Cu-Pb-Zn moving outwards.

**Keywords:** vein-type Cu-Pb-Zn mineralization; hydrothermal alteration geochemistry; mass-balance calculation; Eğrigöz granitoids; Kütahya; Turkey

## 1. Introduction

The metallogenic belt in Turkey lies within the Anatolian tectonic belt which is a part of the larger Tethyan-Eurasian metallogenic belt (TEMB). TEMB was formed during Mesozoic and Early Cenozoic times [1]. In the western part of this belt, mineralization was controlled by extensional events that took place after the closure of the NeoTethys [1]. It is linked with the subduction of Neothyan oceanic crust remnants beneath the Anatolian plate along the Aegean-Cyprean Arc. This mineralization is also related to the Oligocene-Miocene/Pliocene calc-alkaline magmatic activity during post-collision continent-continent setting and includes Pb-Zn, Sb, As, and Au-Cu deposits [1]. Kuşcu *et al.* [2] reported four different varieties of mineral deposits occurring in the western TEMB: (1) low and high

sulfidation epithermal deposits (Au and Au-Ag), (2) mesothermal (Cu-Pb-Zn), (3) skarn (Fe-Cu and Pb-Zn), and (4) porphyry Cu deposits.

The Eğrigöz granitoid is located in western Anatolia (NW Turkey) and is a Cenozoic magmatic intrusion associated with the Hellenic subduction zones [3–6]. It represents the largest regionally exposed NNE-trending pluton, covering ~400 km$^2$, and it syn-tectonically intrudes into the northern Menderes Massif (foliated metagranites, gneissic granites, and microgranites) and Tavşanlı zone (blueschist/ultramafic belt) [7] (Figure 1a,b). Its granitic rocks occur in different textural varieties, ranging from microgranites chilled along the peripheral contact with Menderes Massif into a coarser holocrystalline character moving inward [8]. They are also formed by partial melting of mafic, lower crustal rocks during post-collisional extensional tectonics in the region [9] and are coeval to Oligo-Miocene granitoids in the central Aegean Sea region. Altunkaynak *et al.* [6] reported a SHRIMP U-Pb zircon age of emplacement of Eğrigöz granitoids at 19.48 ± 0.29 Ma, while the $^{39}Ar/^{40}Ar$ dating of biotite and hornblende separated from these rocks is of 19.0 ± 0.1 Ma and 18.9 ± 0.1 Ma, respectively. The mineralization associated with the Eğrigöz granitoids includes Fe skarn deposits [10,11], where they are distributed along the border of this intrusion and within other metamorphic rocks at the Çatak and Küreci area in the north, and the Kalkan and Karaağıl skarn in the south.

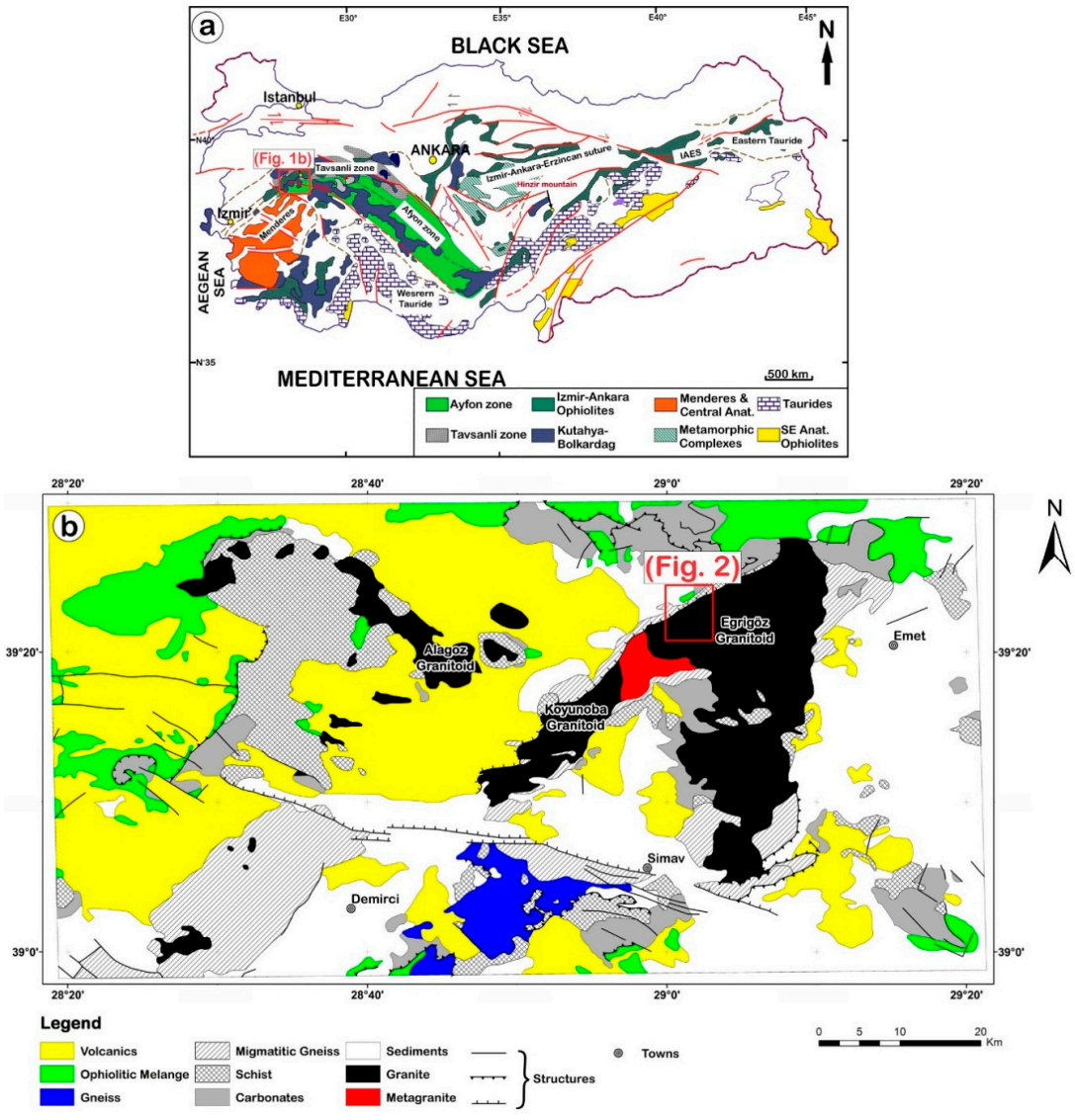


**Figure 1.** (**a**) Map of Turkey [2,12]; (**b**) Area around Eğrigöz granitoids at the northern Menderes core complex (MCC) [13,14].

This paper focuses on the vein-type Cu-Pb-Zn mineralization in Eğrigöz granitoids with special reference to the petrology and geochemistry of different hydrothermal alteration zones around the mineralized veins in the mine area by applying the mass and volume gains and losses of chemical components during the alteration process, which reflect chemical exchanges between wall rocks and hydrothermal fluids [15–19]. The geological and petrographic studies determine the key features of host rocks, mineralogical changes and alteration zones related to the Cu-Pb-Zn mineralization.

## 2. Materials and Methods

Field work was carried out during a number of field workings to collect rock samples representing the different rock units and mineralization types. Fifty thin-sections and polished sections were examined petrographically. Whole-rock major and trace element analyses were conducted for 23 rock samples in the Geochemistry Research Laboratories of Istanbul Technical University (ITU/JAL). The samples were pulverized using a Tungsten Carbide milling device. Major elements of the samples were analyzed by using a BRUKER S8 TIGER model X-ray Fluorescence spectrometer (XRF) (Istanbul Technical University, Istanbul, Turkey) with a wavelength range from 0.01–12 nm. Trace elements were analyzed by using Inductively Coupled Plasma-Mass Spectrometry (ICP-MS) ELAN DRC-e Perkin Elmer model (Istanbul Technical University). Approximately 100 mg powder sample was digested in two steps. The first step was completed with 6 mL 37% HCl, 2 mL 65% $HNO_3$ and 1 mL 38%–40% HF in a pressure- and temperature-controlled Teflon beaker using Berghoff Microwave™ at an average temperature of 180 °C. The second step was completed with the addition of 6 mL 5% Boric acid solution. The remaining solution sample was analyzed by ICP-MS instrument. Normative mineral abundances were calculated from the major elements analyses and plots of elements were created using the igneous petrology software® Igpet (version 2.3) [20]. GEOISO-Windows™ program [21] was used for calculation and plotting of mass balance/volume change by determination of the absolute mobility of elements using equations from Gresens [15] and isocon diagrams of Grant [16,17].

## 3. Geology of the Study Area

The study area is located about 50 km north of the Simav district (Kütahya-Turkey) (Figure 1b) in the Tavşanlı zone of the Kütahya-Bolkardağ Belt (KBB) at the northern margin of the Tauride-Anatolide platform (TAP). It represents parts of the northern Menderes core complex (MCC) in the Anatolian tectonic belt (Figure 1b). This area is near Sudöşeği village at the southwest of Kütahya in the Korucuk region along the Dağardı district (Figure 2). Detailed field mapping reveals that it comprises Precambrian mylonitic biotite gneisses (Menderes massif), Paleozoic metamorphic rocks (mica schist, chlorite schist, calc-schist and marble), Jurassic limestone, and Cretaceous Dağardı ophiolite mélange. These rocks were intruded by the Miocene Eğrigöz granitoids (Figure 2).

*Precambrian mylonitic biotite gneisses* represent the oldest rocks formed in the base of the northern Menderes core complex (MCC) (Figure 2). These rocks are intruded by the Eğrigöz granitoids and are highly mylonitized as a result of shearing (Figure 3a). They are medium- to coarse-grained, whitish-grey in color, and show well-developed gneissic textures. They consist essentially of biotite and recrystallized quartz-feldspar aggregates with minor opaque minerals (Figure 3a). K-feldspar is represented by microcline microperthite that formed large crystals surrounded by biotite lathes and quartz. Zircon occurs as an accessory mineral, forming high relief anhedral crystals (Figure 3b).

*The Paleozoic metamorphic rocks* that surround the Eğrigöz granitoids contain mica schist, chlorite schist, calc-silicate schist, and marble. They are affected by low-, moderate- and high-grade metamorphism [22]. The marble that appears in study area is fine- to medium-grained, grayish in color, and composed essentially of carbonate (calcite and magnesite, ~80 vol. %), K-feldspar, and quartz (Figure 3c). The marble is occasionally cut by small quartz veinlets that are either parallel or cross-cutting each other (Figure 3d).

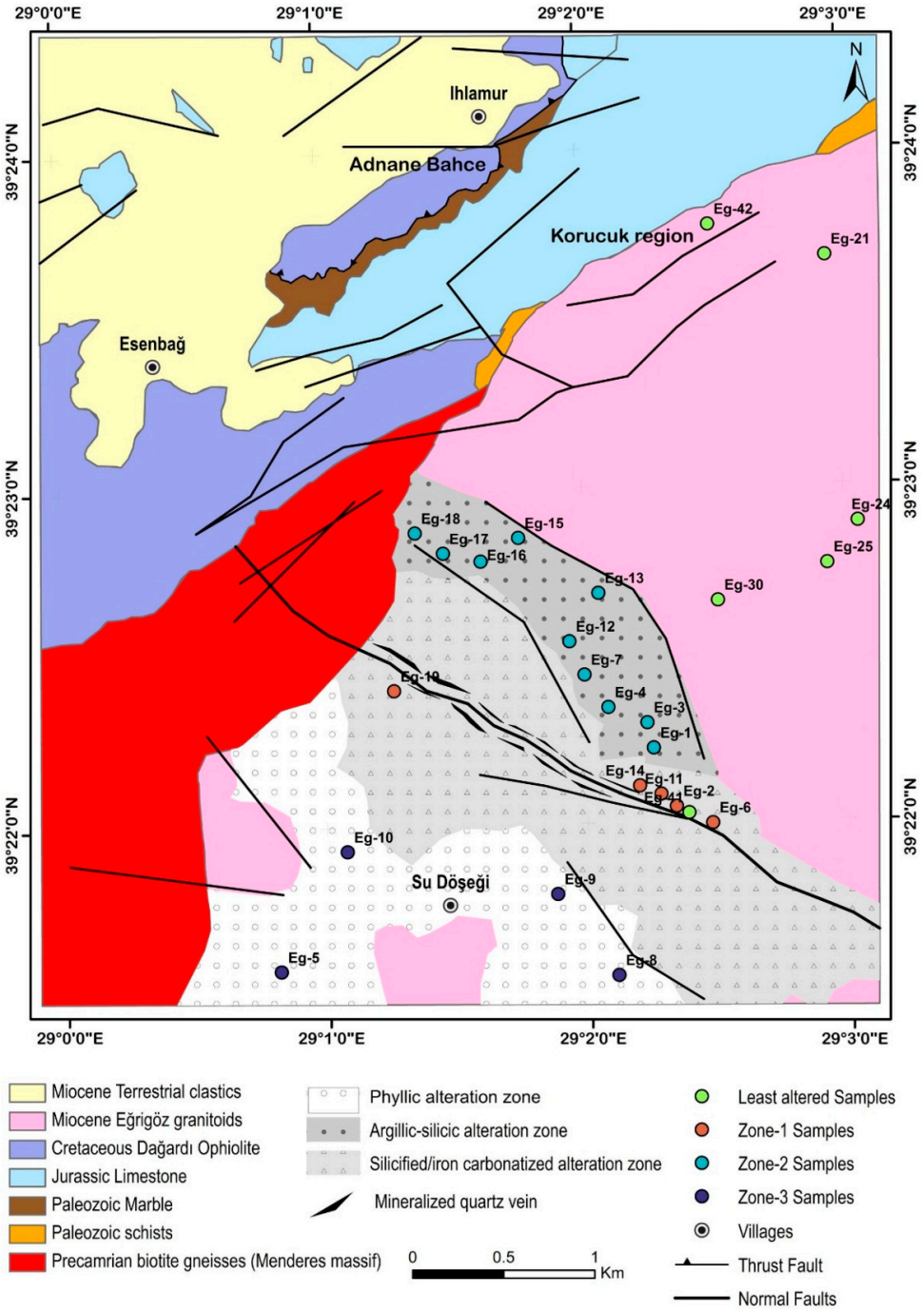


**Figure 2.** Geologic map of the study area (simplified after [22,23]).

*The Cretaceous Dağardı mélange* represents the southernmost continuation of the Tavşanlı Zone [24] occurring in the northwestern part of the study area. It was emplaced onto the Tauride-Anatolide Platform during the Late Cretaceous period and formed a belt of allochthonous assemblages sourced from the Neotethyan Izmir-Ankara-Erzincan Ocean [24]. Petrographically, the Dağardı mélange is represented by tremolite-actinolite schists in the Adnan Bahce area. These rocks are fine-grained, foliated and greenish-grey in color, and they consist of bundles of actinolite crystals embedded in a schistose groundmass of tremolite, actinolite, and quartz with pyroxene relics and opaque minerals (Figure 3e). Tremolite is the dominant amphibole group mineral, and it is commonly colorless, forming subhedral fibrous crystals with a preferred orientation parallel to the main foliation trend. Actinolite is

characterized by a pale green color with parallel arrangement of elongated small prisms. These rocks are cut by quartz and carbonate veinlets that are parallel to the main foliation trend (Figure 3e,f).

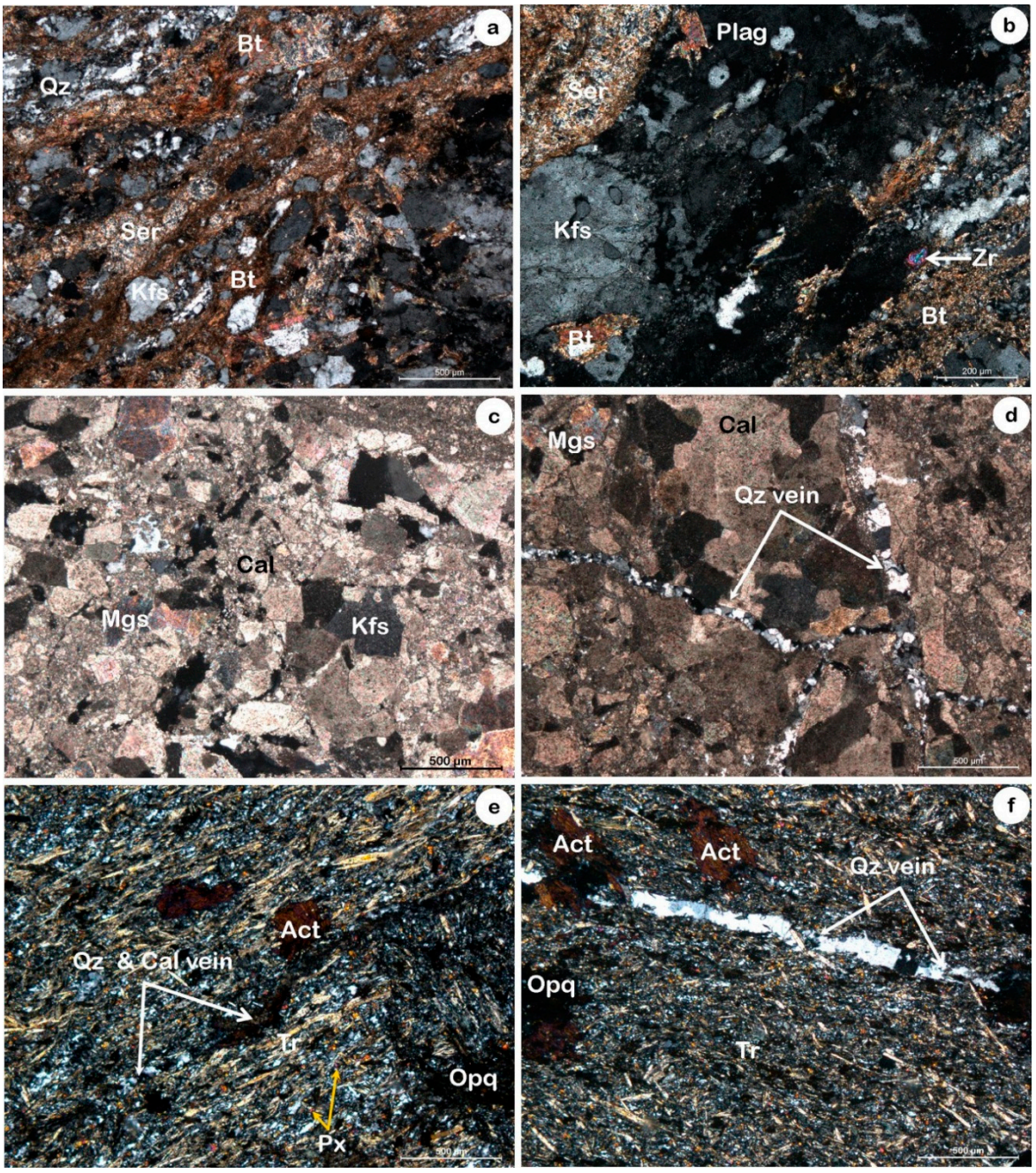


**Figure 3.** (**a**) Streaks of highly deformed and recrystallized quartz and feldspar with biotite as a result of mylonitization in biotite gneiss; (**b**) K-feldspar, plagioclase and biotite with zircon in biotite gneiss; (**c**) Carbonate (calcite and magnesite) with lesser amounts of K-feldspar, and quartz in marble of Paleozoic metamorphic rocks; (**d**) Small quartz veinlets cross-cut each other in marble; (**e**) Bundles of actinolite crystals embedded in a schistose groundmass of tremolite, and quartz in tremolite-actinolite schist of Dağardı mélange; (**f**) Quartz and carbonate veinlets are parallel to the main foliation trend of tremolite-actinolite schist. Abbreviations: actinolite (Act), biotite (Bt), calcite (Cal), K-feldspar (Kfs), magnesite (Mgs), opaque mineral (Opq), plagioclase (Plag), pyroxene (Px), quartz (Qz), sericite (Ser), tremolite (Tr), and zircon (Zr).

*The Eğrigöz granitoid* is the largest exposed pluton in western Anatolia that intruded into the rocks of the northern Menderes Massif (Figure 1b). The northern part of this pluton covers a wide area of the study area at the eastern and southern sides (Figure 2). Based on the modal analyses, these rocks are in monzogranitic and quartz monzonitic compositions (Figure 4). Monzogranitic rocks consist of quartz (~25 vol. %) and K-feldspar (orthoclase and microperthite, ~45 vol. %) with a minor amount of plagioclase (~35 vol. %), biotite (~5 vol. %), and minor sericite, zircon and opaques (~1 vol. %) (Figure 5a). Plagioclase (albite to oligoclase) forms colorless, subidiomorphic, elongated and tabular crystals, with distinct lamellar twinning and sometimes zoning. Sericite is an alteration mineral occurring after K-feldspar and oligoclase (Figure 5b). Quartz monzonitic rocks contain quartz (~15 vol. %) and are accompanied by K-feldspar (orthoclase- and microcline-microperthite; (~35 vol. %)), oligoclase (~35 vol. %), and biotite with some opaque minerals (Figure 5c). Some samples contain minor clinopyroxene (Figure 5d), hornblende (Figure 5e) and zircon enclosed in the biotite crystal (Figure 5f).

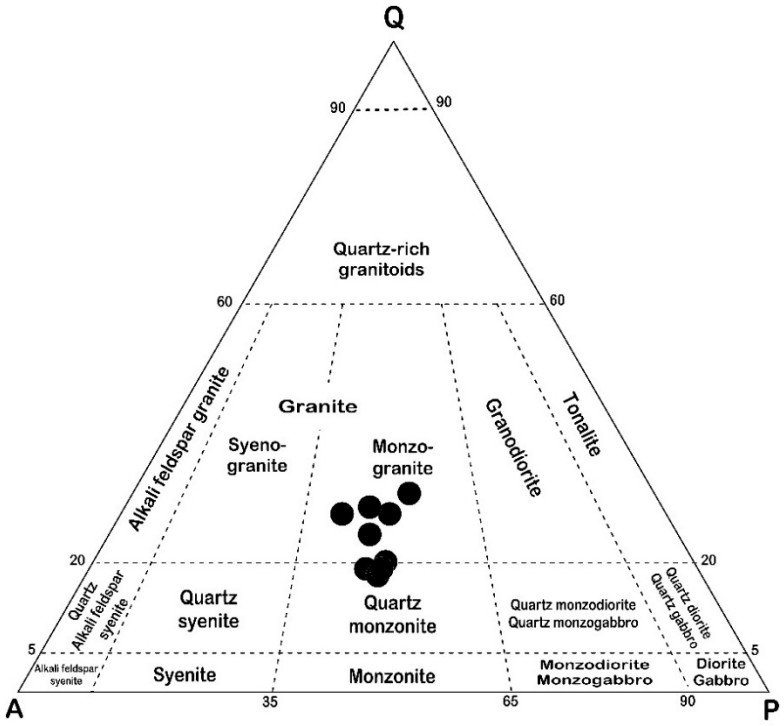


**Figure 4.** Classification of Eğrigöz granitoids, based on modal mineralogy [25], Q = quartz; A = Alkali feldspar; P = Plagioclase.

## 4. Results and Discussion

### *4.1. Cu-Pb-Zn Mineralization and Associated Hydrothermal Alterations*

Cu-Pb-Zn mineralization hosted by the Eğrigöz granitoids is closely associated with an intense hydrothermal alteration that was controlled by NW-SE-trending faults within brecciation, quartz stockwork veining, and brittle fracture zones (Figure 2). The normal faults cut through this pluton at the southern part of the study area and are nearly parallel to the direction of Simav graben (NWN-ESE). In addition, these faults were considered to be conduits for the transport of ore-bearing fluids to structurally favorable sites for the deposition of ore minerals [26]. The mine area extends approximately 600 m along this fault zone in the valley (NW-SE direction). Oyman *et al.* [10] and Uğurcan and Oyman [11] stated that Fe-skarn deposits were formed along the contact of Eğrigöz granitoids with Paleozoic metamorphic rocks (mica schist, chlorite schist, calc-silicate schist, and marble) along its

northern and southern borders. The studied Cu-Pb-Zn mineralization is found locally as vein-type deposits near these skarn deposits, and is controlled by faulting which post-dates the intrusion. It is characterized by a retrograde alteration forming K-silicate and sericitic alterations (sericite + chlorite + kaolinite ± tremolite ± calcite).

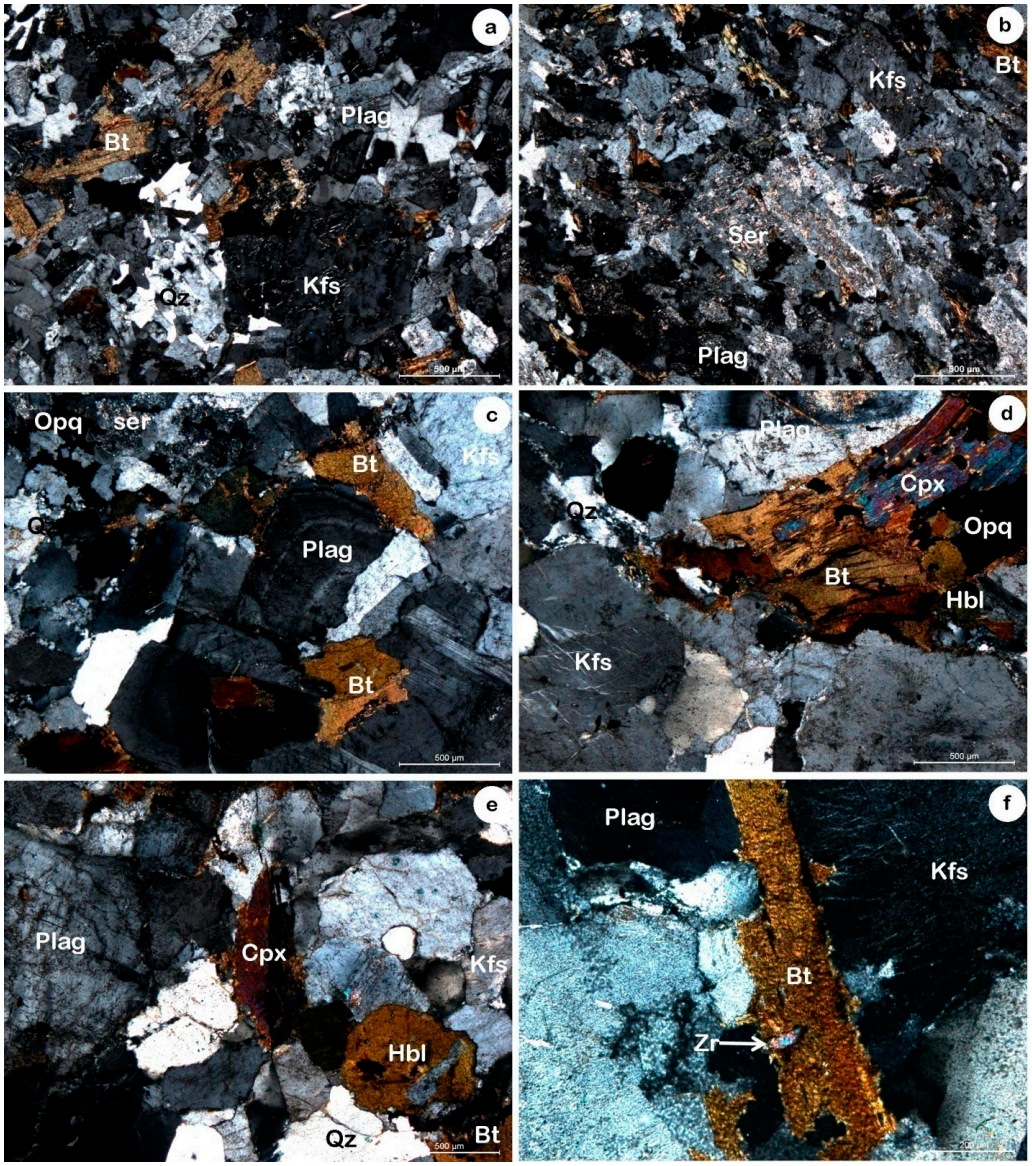


**Figure 5.** Photomicrographs of Eğrigöz granitoids: (**a**) Quartz, K-feldspar, plagioclase with biotite in Eğrigöz monzogranite; (**b**) Sericitic alteration after K-feldspar and plagioclase in monzogranite; (**c**) Zoned plagioclase with quartz, K-feldspar and biotite in Eğrigöz quartz monzonite; (**d**) and (**e**) Minor clinopyroxene and hornblende with containing biotite and zircon in quartz monzonite; (**f**) Zircon enclosed in biotite in quartz monzonite. Abbreviations: biotite (Bt), clinopyroxene (Cpx), hornblende (Hbl), K-feldspar (Kfs), opaque mineral (Opq), plagioclase (Plag), quartz (Qz), sericite (Ser), and zircon (Zr).

### 4.1.1. Hydrothermal Alterations

Variable types and styles of hydrothermal alterations are observed around the fault/shear zone in the Eğrigöz granitoids. Three main alteration zones with gradual boundaries are distinguished based on the field relationships, and geological and petrographic data. Zone 1: silicified/iron carbonatized

alterations (quartz-sulfide-carbonate ± albite) occurred around ore veins and shear zones; zone 2: argillic-silicic alterations (quartz-sulfide ± kaolinite ± sericite ± chlorite), and zone 3: phyllic alterations (sericite/muscovite-quartz-sulfide ± carbonate ± tremolite).

*The silicified/iron carbonatized alteration zone (zone 1)* envelops ore veins and/or shear zones in the mine area and is characterized by yellowish/brownish or reddish colors (Figure 6a,b). As this zone is near the fault zone, it is highly affected by brecciation (Figure 6c). Based on ore mineralogical studies, it has a high amount of chalcopyrite and pyrite with the alteration minerals (Figure 6d).

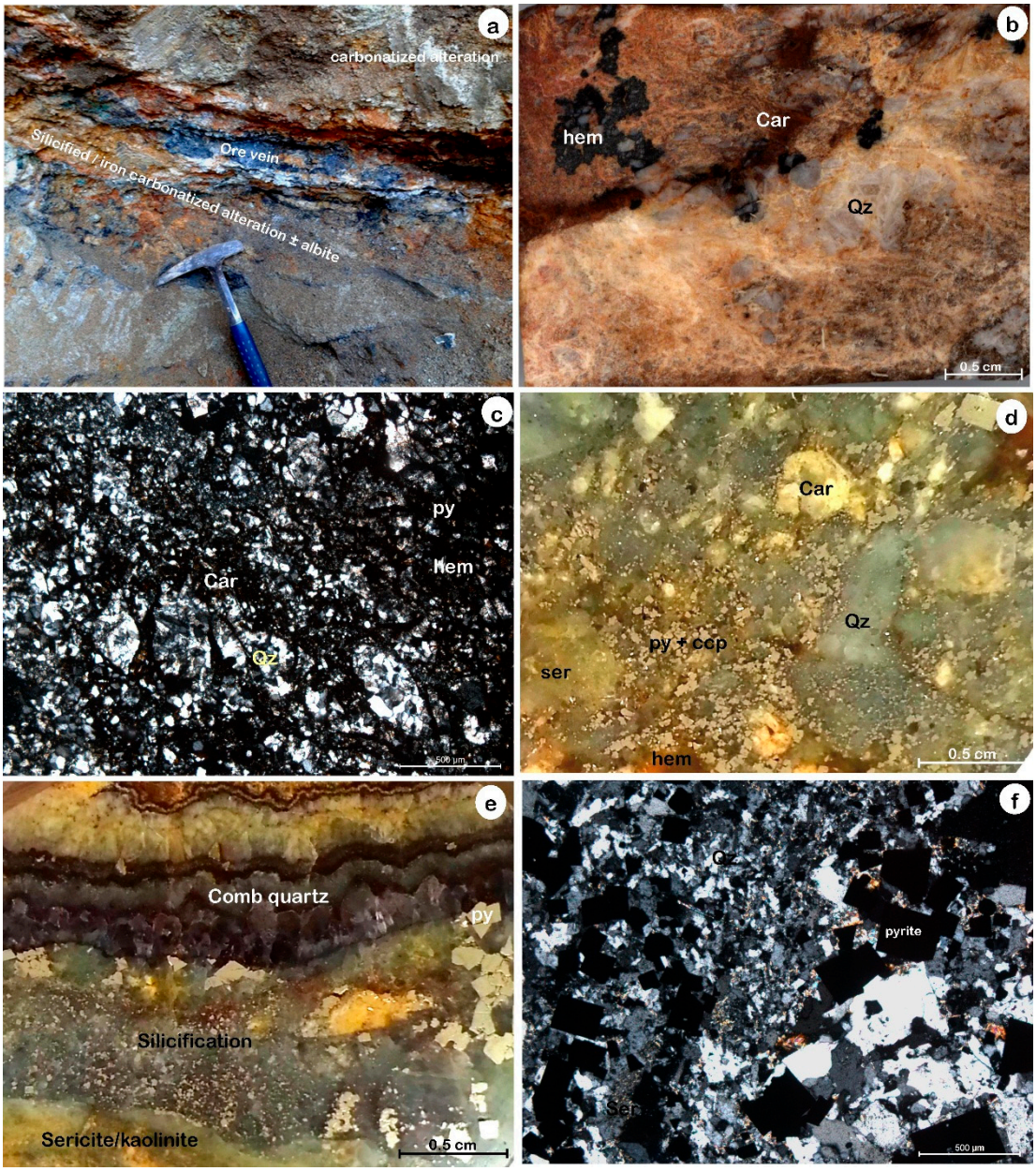


**Figure 6.** (**a**) Silicified/iron carbonatized alteration ± albite; (**b**) Reflected light, centimeter-scale view of carbonatization alteration with quartz in zone 1; (**c**) Brecciation of quartz filled by carbonate and sulfide (pyrite) in zone 1; (**d**) Carbonate, quartz and sulfide (pyrite and chalcopyrite) with sericite in zone 1; (**e**) Reflected light, centimeter-scale view of comb-textured quartz crystals within wall rock (sericitized, kaolinitized and silicic) in zone 2; (**f**) Quartz and sulfide minerals with sericite in zone 2. Abbreviations: carbonate (Car), chalcopyrite (ccp), hematite (hem), pyrite (py), quartz (Qz), and sericite (Ser).

*The argillic-silicic alteration zone (zone 2)* is in contact between the northern border of zone 1 and the Eğrigöz granitoids. It is represented by rocks enriched in quartz and sulfide minerals with kaolinite, sericite, and chlorite (Figure 6e,f). Quartz veins are characterized by the comb-textured infilling of quartz crystals growing out from a wall rock (Figure 6e). The mineralization in this zone is situated within the contact with quartz veins and alteration minerals (Figure 7a) enriched in chalcopyrite and sphalerite with pyrite.

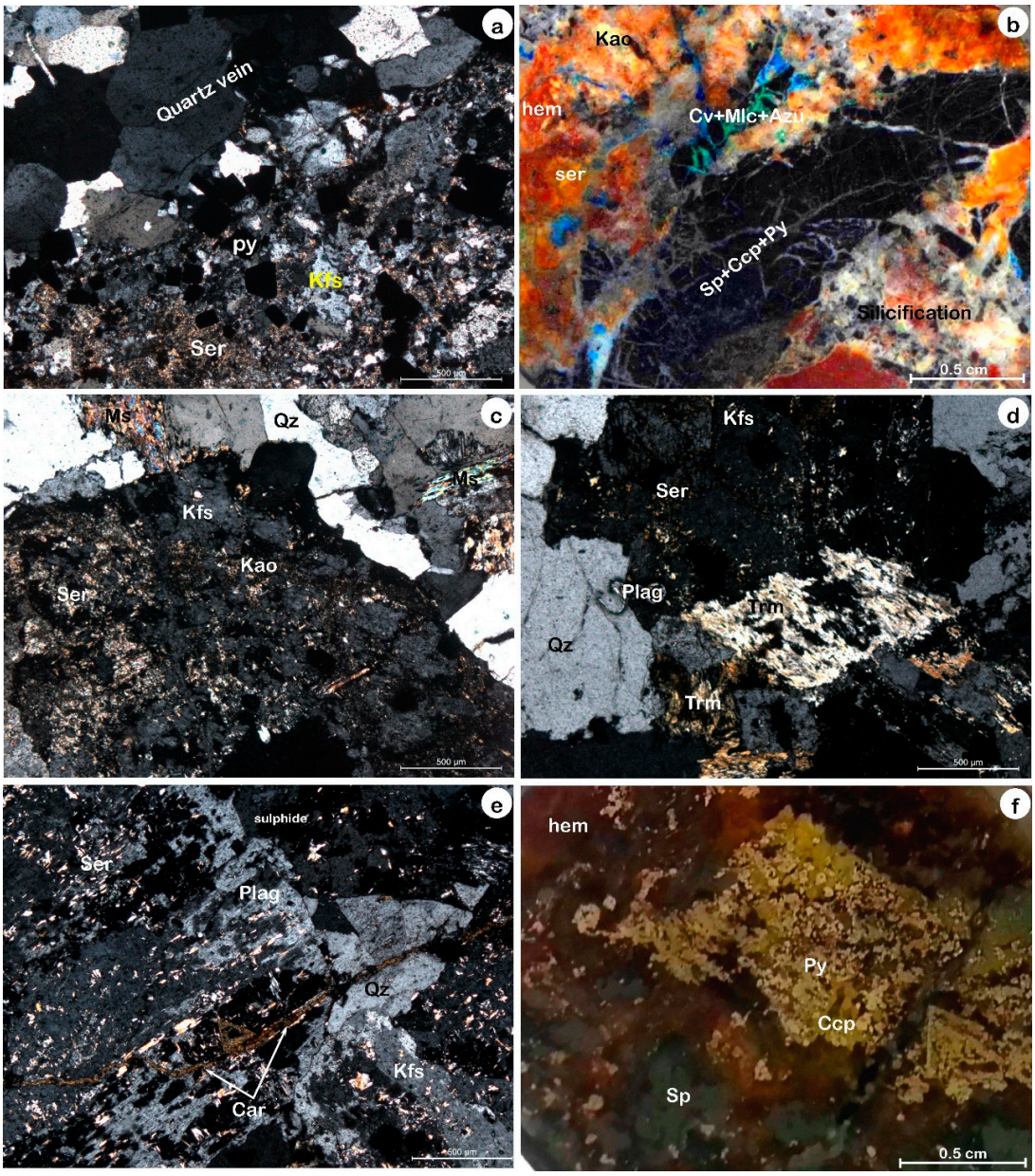


**Figure 7.** (**a**) Enriched mineralization at contact with quartz veins and sericitic alteration in zone 2; (**b**) Reflected light, centimeter-scale view shows phyllic alteration with sulfide in zone 3; (**c**) Kaolinite and sericite/muscovite with quartz in zone 3; (**d**) Tremolite and sericite alteration in zone 3; (**e**) Carbonate veinlets traversed the altered rocks; (**f**) Reflected light, centimeter-scale view of pyrite, chalcopyrite, sphalerite, and hematite in zone 3. Abbreviations: azurite (Azu), carbonate (Car), chalcopyrite (Ccp), covellite (Cv), hematite (hem), K-feldspar (Kfs), kaolinite (Kao), malachite (Mlc), muscovite (Ms), plagioclase (Plag), pyrite (Py), quartz (Qz), sericite (Ser), and sphalerite (Sp).

*The phyllic alteration zone (zone 3)* is the outer zone and is characterized by preferential replacement of the original K-feldspar and/or plagioclase-biotite by sericite/muscovite-kaolinite-carbonate (Figure 7b,c). Some samples have tremolite (Figure 7d), traversed by a few carbonate veinlets (Figure 7e). This zone has a high amount of chalcopyrite, sphalerite, and galena with pyrite (Figure 7b,f).

#### 4.1.2. Ore Mineralogy

The ore mineralogy includes chalcopyrite, sphalerite, galena, pyrite, covellite, malachite, and azurite. These ore minerals are disseminated in the alteration zones, as well as at the contact between quartz veins and highly altered granite. Gangue minerals include quartz, mica, and calcite.

Chalcopyrite is characterized by a brassy yellow color in air with high reflectance, weak bireflectance and weak anisotropy. It occurs as fine- to medium-grained, anhedral to subhedral crystals (up to 4 mm in grain size) disseminated in gangue quartz and altered zones within quartz veins and host rocks. It is associated with pyrite, sphalerite, and galena (Figure 8a) and occurs as inclusions in sphalerite as chalcopyrite exsolution (Figure 8b). Also, it is partly replaced by sphalerite and poikilitically trapped within massive pyrite. Chalcopyrite crystals are slightly corroded along their cracks replaced by covellite (Figure 8c). They often display various oxidation products with covellite and goethite in the weathered areas. Sphalerite is the second-most abundant sulfide mineral. It is characterized by grey color with low reflectance and isotropism and occurs as coarse anhedral grains (up to several centimeters in size) in the main vein as well as in the altered host rocks associated with copper minerals. It is always found close to chalcopyrite and covellite (Figure 8d) with ragged edges and fractures. Galena occurs disseminated in quartz-veined altered rocks either as subhedral to anhedral grains and massive, or as inclusions within sphalerite. It is characterized by white to whitish-grey colored grains with triangular cleavage pits and it sharply cuts across chalcopyrite and sphalerite (Figure 8e). Inclusions of chalcopyrite are found within galena as irregular veinlets. Pyrite shows a whitish-yellow color with high reflectivity and forms idiomorphic crystals associated with chalcopyrite, sphalerite, and galena. It occurs as irregular and corroded massive aggregates scattered in quartz veins of the host rock. Pyrite displays progressive stages of alteration to goethite (Figure 8f). Covellite is characterized by strong blue color with orange to reddish-brown anisotropism and is derived from the alteration of chalcopyrite along their fractures or partial and/or complete alteration (Figure 9a,b). Malachite occurs as aggregates in association with chalcopyrite, sphalerite, and azurite and appears green in color in cross-polarized light and grey in color with low reflectance in plane-polarized light (Figure 9c,d). Azurite, like malachite, is associated with chalcopyrite and sphalerite and occurs in supergene weathered deposits, and it has a blue color (Figure 9c,d). Fe-oxides and hydroxides that are represented by hematite and goethite occur mainly as alteration products replacing the Fe-bearing sulfide minerals in quartz veins and alteration zones. They occur as porous colloform bands with radiating fine fibers and/or massive crystal aggregates associated with pyrite (Figure 8f).

Paragenetic relationships appear in three stages of mineralization: pre-ore, ore, and supergene. Each stage is characterized by unique mineral assemblages (Figure 10). The pre-ore stage has disseminated euhedral pyrite and quartz, observed as a large anhedral crystal matrix. The main hydrothermal stage has sphalerite predated by galena and chalcopyrite. During this stage, a second type of quartz was deposited as small crystals forming thin veinlets. The supergene post-ore assemblage consists of covellite, malachite, azurite, and Fe-oxides and -hydroxides.

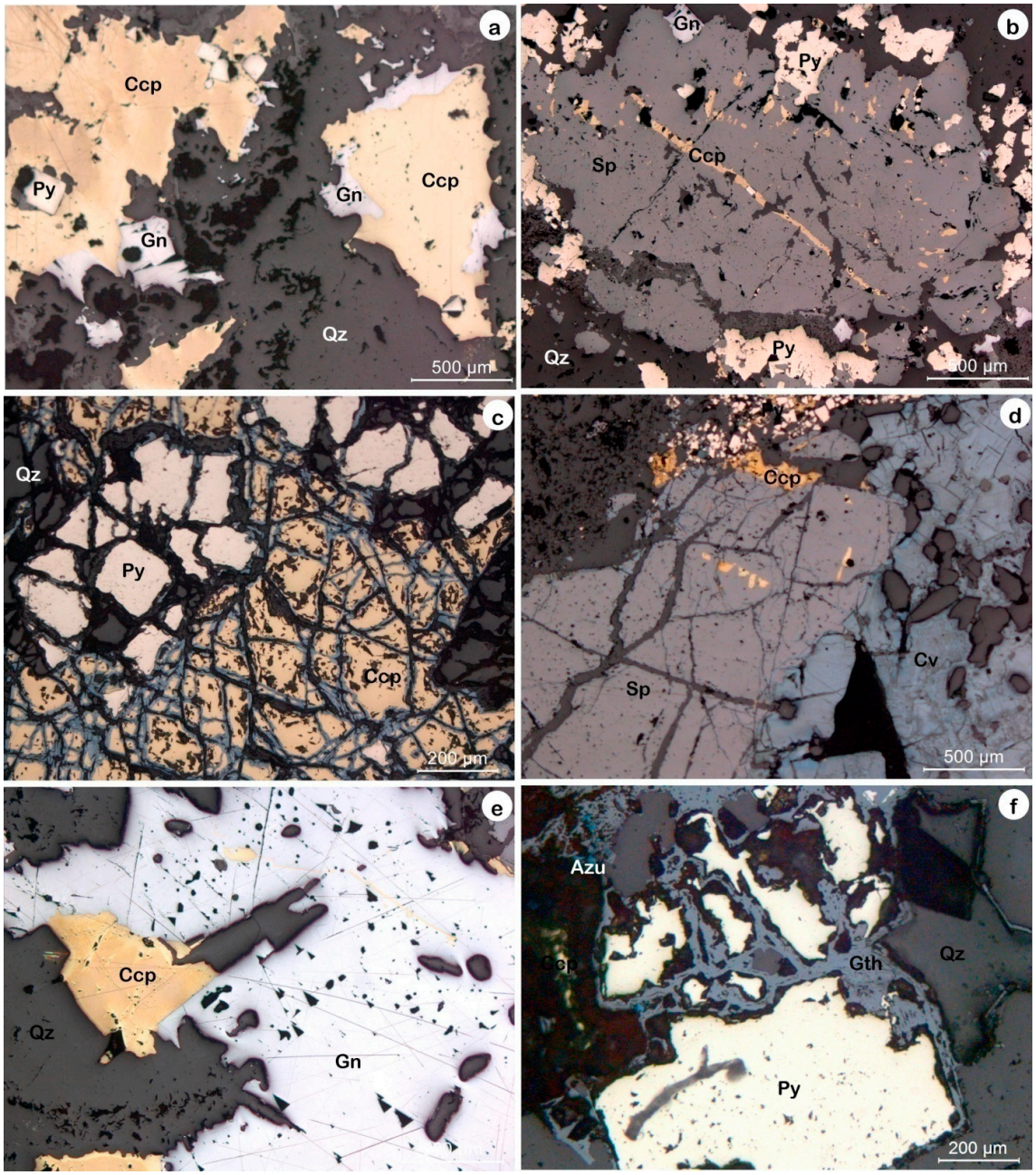


**Figure 8.** Photomicrographs of reflected light microscopy: (**a**) Chalcopyrite associated with pyrite and galena in a quartz vein; (**b**) Inclusions of chalcopyrite in sphalerite as chalcopyrite disease; (**c**) Slightly corroded along chalcopyrite cracks replaced by covellite; (**d**) Sphalerite with chalcopyrite, covellite and pyrite; (**e**) Galena with triangular cleavage pits associated with chalcopyrite in quartz vein; (**f**) Alteration of pyrite to goethite with azurite. Abbreviations: azurite (Azu), chalcopyrite (Ccp), covellite (Cv), galena (Gn), goethite (Gth), pyrite (Py), sphalerite (Sp), and quartz (Qz).

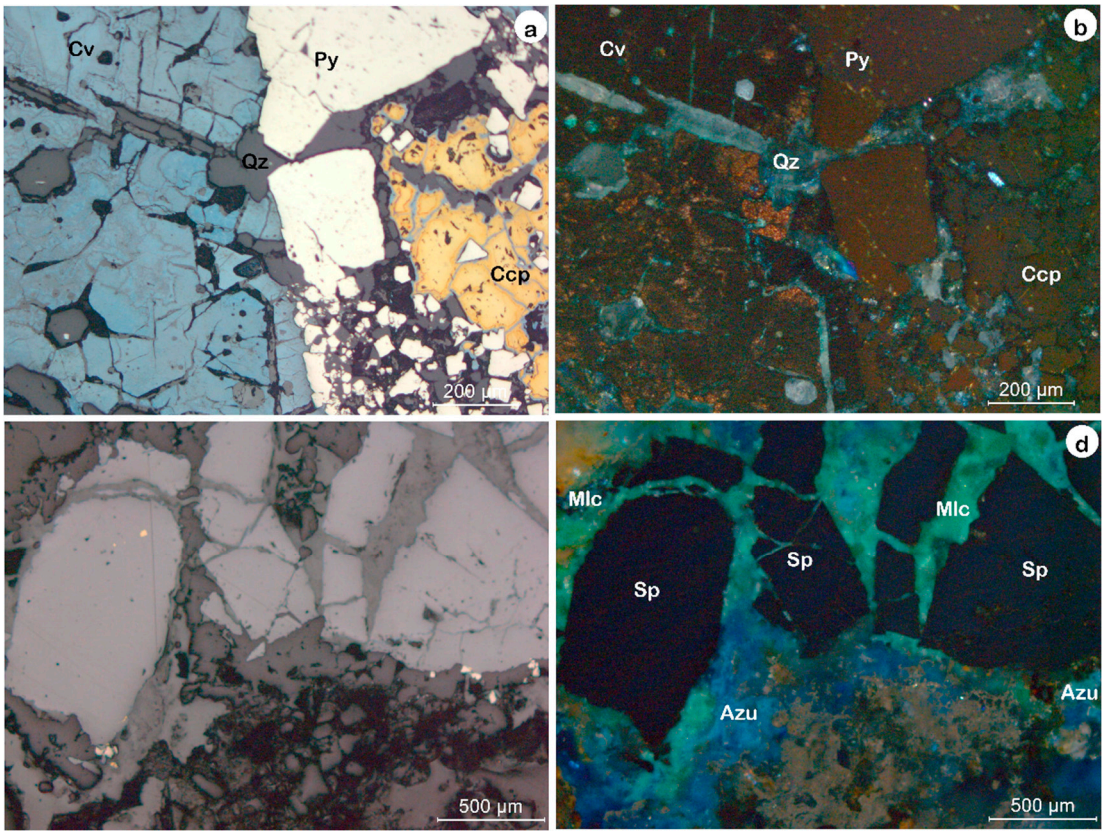


**Figure 9.** Photomicrographs of reflected light microscopy: (**a**) Covellite is an alteration product after chalcopyrite; (**b**) The same as Figure 7a but in cross-polarized light (XPL); (**c**) Aggregates of malachite (green) and azurite (blue) associated with sphalerite; (**d**) The cross-polarized light (XPL) of Figure 7c. Abbreviations: azurite (Azu), chalcopyrite (Ccp), covellite (Cv), malachite (Mlc), pyrite (Py), quartz (Qz), and sphalerite (Sp).

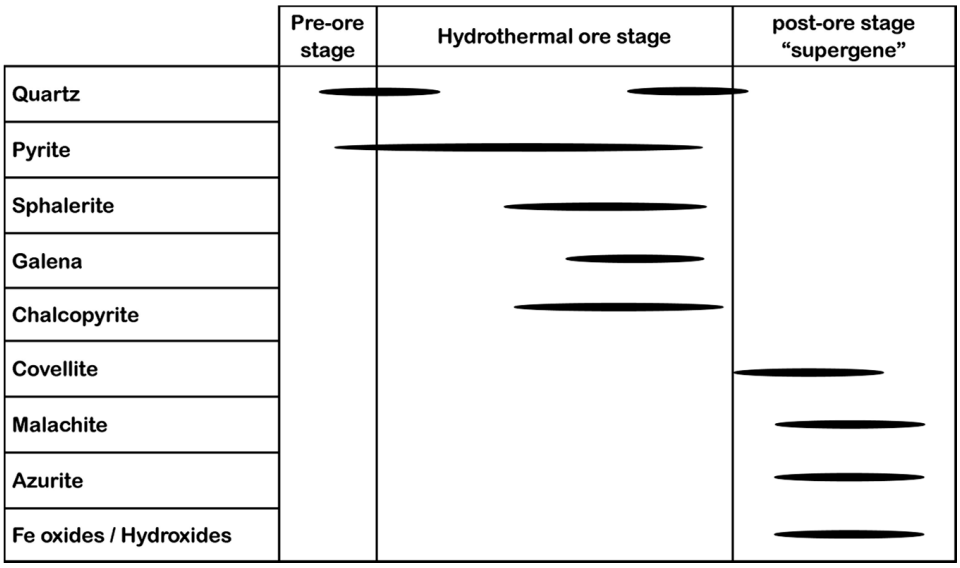


**Figure 10.** Paragenetic sequence of quartz, sulfide minerals, and supergene minerals as defined by mineral assemblages.

### *4.2. Geochemical Characteristics*

The granitoid rocks are divided into least-altered and altered rocks. The altered rocks have spatially associated with Cu-Pb-Zn mineralization developed along NW-SE fault zones in the northern part of the Eğrigöz granitoids. Six representative samples were collected from the least-altered granitoid rocks and 17 representative samples were collected from the altered rocks. Each was analyzed for major and trace elements (Tables 1 and 2).

**Table 1.** Major and trace elements contents of Eğrigöz granitoids at the Tavşanlı area.

| Sample ID | Detection Limit | Eg-21 | Eg-23 | Eg-25 | Eg-30 | Eg-41 | Eg-42 |
|---|---|---|---|---|---|---|---|
| Major elements (wt %) | | | | | | | |
| $SiO_2$ | 0.016 | 67.2 | 66.8 | 66.0 | 65.0 | 65.9 | 68.8 |
| $Al_2O_3$ | 0.026 | 15.0 | 15.1 | 15.7 | 15.1 | 15.2 | 15.4 |
| $Fe_2O_3$ | 0.001 | 2.9 | 2.9 | 3.2 | 4.1 | 3.5 | 1.2 |
| MgO | 0.060 | 1.3 | 1.2 | 1.3 | 1.2 | 1.0 | 1.1 |
| CaO | 0.001 | 2.5 | 2.9 | 3.2 | 3.3 | 2.9 | 2.4 |
| $Na_2O$ | 0.120 | 3.6 | 3.5 | 3.6 | 3.5 | 3.3 | 3.9 |
| $K_2O$ | 0.001 | 5.4 | 5.3 | 4.7 | 5.3 | 5.7 | 5.2 |
| $TiO_2$ | 0.001 | 0.5 | 0.5 | 0.5 | 0.3 | 0.5 | 0.2 |
| $P_2O_5$ | 0.012 | 0.2 | 0.2 | 0.2 | 0.2 | 0.3 | 0.1 |
| MnO | 0.001 | 0.05 | 0.08 | 0.07 | 0.02 | 0.05 | 0.03 |
| $CO_2$ | - | 0.04 | 0.35 | 0.24 | 0.33 | 0.13 | 0.19 |
| $SO_2$ | 0.002 | 0.01 | 0.01 | 0.01 | 0.10 | 0.11 | 0.02 |
| LOI | - | 0.8 | 1.1 | 1.0 | 2.0 | 1.6 | 1.7 |
| Trace elements (ppm) | | | | | | | |
| As | 10 | - | - | - | 80 | 10 | 20 |
| Ba | 24 | 1260 | 1190 | 1200 | 1350 | 1030 | 300 |
| Co | 9 | 20 | 30 | 35 | 10 | 20 | 15 |
| Cs | - | - | 188 | 128 | 6 | 8 | 7 |
| Cu | 1 | 3 | 5 | 5 | 61 | 12 | 1 |
| Ga | 6 | 15 | 15 | 16 | 15 | 16 | 15 |
| Nb | 6 | 14 | 15 | 14 | 14 | 15 | 14 |
| Ni | 6 | 8 | 6 | 9 | 11 | 7 | 7 |
| Pb | 5 | 25 | 31 | 29 | 178 | 36 | 0.7 |
| Rb | 3 | 140 | 140 | 130 | 210 | 170 | 220 |
| S | 20 | 43 | 72 | 53 | 520 | 530 | 110 |
| Sc | 8 | 437 | 252 | 409 | - | 8 | - |
| Sr | 3 | 230 | 220 | 270 | 140 | 220 | 100 |
| W | 8 | 214 | 274 | 357 | - | - | - |
| Y | 3 | 24 | 27 | 29 | 17 | 16 | 28 |
| Zn | 9 | 24 | 36 | 38 | 68 | 37 | 46 |
| Zr | 6 | 140 | 150 | 160 | 140 | 220 | 90 |
| Density | - | 2.7 | 2.7 | 2.7 | 2.7 | 2.7 | 2.7 |
| Quartz | - | 20.3 | 20.9 | 20.3 | 17.8 | 19.1 | 20.9 |
| Orthoclase | - | 32.8 | 31.8 | 28.5 | 32.5 | 34.5 | 31.3 |
| Albite | - | 28.7 | 28.2 | 29.4 | 29.2 | 27.6 | 33.1 |
| D.I. | - | 81.8 | 80.9 | 78.2 | 79.5 | 81.2 | 85.3 |
| $FeO^t$ | - | 2.6 | 2.6 | 2.9 | 3.7 | 3.1 | 1.1 |
| $K_2O/Na_2O$ | - | 1.5 | 1.5 | 1.3 | 1.5 | 1.7 | 1.3 |
| LIL/HFS | - | 7.8 | 6.9 | 6.6 | 9.4 | 4.8 | 3.8 |
| CIA | - | 50.0 | 49.2 | 50.2 | 47.9 | 49.8 | 49.1 |

**Table 2.** Geochemical data of the altered rocks in the study area.

| Sample ID | Detection Limit | Least Altered Mean | Zone-1 | | | | | Zone-2 | | | | | | | | | | Zone-3 | | | |
|---|---|---|---|---|---|---|---|---|---|---|---|---|---|---|---|---|---|---|---|---|---|
| | | | Eg-2 | Eg-6 | Eg-11 | Eg-14 | Eg-19 | Eg-1 | Eg-3 | Eg-4 | Eg-7 | Eg-12 | Eg-13 | Eg-15 | Eg-16 | Eg-17 | Eg-18 | Eg-5 | Eg-8 | Eg-9 | Eg-10 |
| Major elements (wt %) | | | | | | | | | | | | | | | | | | | | | |
| $SiO_2$ | 0.016 | 66.6 | 44.0 | 82.1 | 24.9 | 73.8 | 71.6 | 58.8 | 93.1 | 58.3 | 92.6 | 86.5 | 58.0 | 51.1 | 69.9 | 62.3 | 68.1 | 86.9 | 70.5 | 80.9 | 52.1 |
| $Al_2O_3$ | 0.026 | 15.2 | 1.9 | 1.0 | 2.1 | 0.5 | 13.2 | 3.3 | 1.7 | 6.1 | 1.7 | 1.0 | 3.6 | 3.9 | 10.8 | 6.2 | 15.4 | 5.5 | 8.5 | 5.8 | 10.1 |
| $Fe_2O_3$ | 0.001 | 3.0 | 7.3 | 10.6 | 72.6 | 18.9 | 5.2 | 9.8 | 2.5 | 10.9 | 3.1 | 5.0 | 14.3 | 4.0 | 8.7 | 6.5 | 13.9 | 1.6 | 11.8 | 4.3 | 11.1 |
| MgO | 0.060 | 1.2 | 0.2 | 0.1 | 1.0 | 0.0 | 0.9 | 0.1 | - | 0.1 | - | - | 0.1 | 0.1 | 0.2 | 0.1 | 0.7 | 0.1 | 0.1 | 0.1 | 0.1 |
| CaO | 0.001 | 2.9 | 0.1 | 0.0 | 1.6 | 0.1 | 4.3 | 0.1 | - | 0.1 | 0.1 | - | 0.1 | 0.1 | 0.5 | 0.2 | 2.3 | 0.1 | 0.1 | 0.1 | 0.2 |
| $Na_2O$ | 0.120 | 3.6 | 0.5 | 0.3 | 0.2 | - | 1.6 | 0.2 | 0.2 | 0.8 | 0.1 | - | 0.3 | 0.7 | 0.4 | 0.7 | 3.3 | 0.6 | 0.6 | 0.1 | 0.9 |
| $K_2O$ | 0.001 | 5.3 | - | - | 0.6 | - | 1.8 | - | 0.1 | 1.5 | 0.2 | 0.1 | 0.3 | 0.8 | 2.7 | 1.6 | 4.8 | 2.8 | 4.0 | 2.9 | 3.8 |
| $TiO_2$ | 0.001 | 0.4 | - | - | 0.1 | - | 0.2 | - | - | 0.1 | - | - | - | 0.1 | 0.2 | 0.1 | 0.4 | 0.1 | 0.3 | 0.1 | 0.2 |
| $P_2O_5$ | 0.012 | 0.20 | - | - | 0.06 | 0.01 | 0.04 | - | - | 0.02 | 0.04 | - | 0.03 | 0.03 | 0.12 | 0.06 | 0.14 | 0.04 | 0.06 | 0.03 | 0.10 |
| MnO | 0.001 | 0.05 | 0.30 | 1.32 | 0.04 | 0.46 | 0.10 | 0.25 | 0.01 | 0.11 | - | 0.01 | 0.05 | 0.12 | 0.09 | 0.06 | 0.08 | 0.02 | 0.22 | 0.01 | 0.01 |
| $SO_2$ | 0.002 | 0.04 | 13.67 | 0.24 | - | 1.06 | 3.65 | 9.43 | 10.82 | 18.89 | - | 13.48 | 9.50 | 13.95 | 4.86 | 26.50 | 8.06 | 0.77 | 0.45 | 2.52 | 6.39 |
| LOI | - | 1.4 | 7.1 | 3.3 | - | 3.7 | 4.5 | 6.1 | 2.0 | - | 1.8 | - | 6.4 | 6.5 | 4.7 | 4.1 | 2.3 | 2.1 | 3.1 | 2.5 | 6.7 |
| Trace elements (ppm) | | | | | | | | | | | | | | | | | | | | | |
| As | 10 | 21 | 1417 | 36 | 1815 | 47 | 72 | - | 111 | 307 | 103 | 153 | 237 | 1625 | 111 | 71 | 739 | 55 | 63 | 80 | 373 |
| Ba | 24 | 1050 | - | 30 | 70 | 20 | 950 | 30 | 80 | 520 | 370 | 260 | 180 | 110 | 460 | 440 | 180 | 1040 | 1040 | 660 | 1010 |
| Co | 9 | 20 | 74 | 22 | 81 | 39 | 30 | 80 | 33 | 41 | 38 | 41 | 45 | 60 | 53 | 53 | 78 | 29 | 24 | 29 | 37 |
| Cu | 1 | 15 | 30,100 | 530 | 30,250 | 330 | 540 | 17,000 | 2440 | 8200 | 1900 | 6350 | 56,150 | 32,000 | 1880 | 1680 | 15,700 | 550 | 330 | 1000 | 57,800 |
| Ga | 6 | 15 | - | 10 | - | 7 | 15 | - | 12 | 83 | - | - | 29 | - | 14 | 13 | 66 | - | 7 | - | - |
| Nb | 6 | 14 | - | - | - | - | 8 | - | - | - | - | - | - | 39 | - | - | 54 | - | 7 | - | - |
| Ni | 6 | 8 | 60 | 17 | 115 | 36 | 24 | 40 | - | 26 | - | 7 | 26 | 377,602 | 16 | 10 | 146,869 | - | 21 | 8 | 18 |
| Pb | 5 | 50 | 281,900 | 1400 | 375,500 | 3400 | 1560 | - | 260 | 52,700 | 870 | 9200 | 31,700 | - | 1660 | 1650 | 180 | 1800 | 3040 | 8130 | 65,030 |
| Rb | 3 | 168 | - | - | - | 10 | 78 | - | 3 | - | 3 | - | - | - | 34 | 40 | 14 | 68 | 100 | 77 | 106 |
| S | 20 | 221 | 68,450 | 1200 | - | 5320 | 18,260 | 47,180 | 54,150 | 94,540 | | 67,450 | 47,540 | 69,850 | 24,350 | 132,640 | 40,360 | 3860 | 2260 | 12,600 | 32,000 |
| Sr | 3 | 196 | 22 | 10 | 56 | 10 | 59 | - | 14 | - | - | 10 | 26 | 28 | 24 | 33 | - | 45 | 50 | 46 | 83 |
| Y | 3 | 24 | 306 | 19 | 384 | 32 | 20 | 108 | 3 | 74 | 4 | 16 | 48 | 377 | 9 | 11 | 174 | 8 | 21 | 19 | 98 |
| Zn | 9 | 42 | 188,030 | 6220 | 60,200 | 6150 | 8640 | 61,550 | 3180 | 128,500 | 290 | 1930 | 86,570 | 234,400 | 8500 | 6330 | 256,850 | 860 | 1950 | 2060 | 57,260 |
| Zr | 6 | 149 | 277 | 15 | 376 | 17 | 89 | 113 | 15 | 109 | 17 | 28 | 62 | 353 | 37 | 43 | 188 | 50 | 78 | 56 | 149 |
| Density | - | 2.7 | 3.0 | 2.8 | 4.1 | 3.0 | 2.8 | 3.0 | 2.8 | 3.0 | 2.7 | 2.9 | 3.0 | 3.4 | 2.9 | 3.0 | 3.1 | 2.7 | 2.8 | 2.8 | 3.0 |
| CIA | - | 49.4 | 65.6 | 61.0 | 37.5 | 74.2 | 52.2 | 85.9 | 80.8 | 67.6 | 90.5 | 81.9 | 81.0 | 67.6 | 74.1 | 68.4 | 52.2 | 58.2 | 63.2 | 63.7 | 65.6 |

4.2.1. Geochemistry of Least-Altered Rocks

The least-altered monzogranitic and quartz monzonitic Eğrigöz granitoids have $SiO_2$ contents ranging from 64.9 to 68.8 wt % with an average differentiation index (D.I. = Qz + Ab + Or) of 81.2%. They have relatively high K contents with $K_2O/Na_2O$ ratios ranging from 1.3 to 1.7. On the AFM (Alkalis-$FeO^t$-MgO) ternary diagram (Figure 11a) as defined by Irvine and Baragar [27], and the data points fall in the calc-alkaline field, being relatively rich in total alkali contents, coinciding with the extensional trend of Petro *et al.* [28]. The alumina saturation index (ASI = A/CNK = molar $Al_2O_3/(CaO + Na_2O + K_2O)$) of the studied samples of the granitoid rocks is mostly less than 1.0. Therefore, these samples are classified as metaluminous in the A/CNK *versus* A/NK diagram [29] (Figure 11b). In the ternary $Na_2O$-CaO-$K_2O$ diagram [30], the Eğrigöz granitoids are plotted in the granite and quartz monzonite field (Figure 11c). This is consistent with the petrographical classification of these based on modal analysis. According to the Mol. $Al_2O_3/(CaO + Na_2O + K_2O)$-Rb/Sr diagram [31], these rocks are plotted within the I-type field (Figure 11d). Harris *et al.* [32] used the Rb/Zr *versus* $SiO_2$ diagram to differentiate between two types of granites that are related to Group II and Group III. Group II granites are peraluminous syn-orogenic and similar to the S-type granites of Chappell and White [31] derived from two sources: hydrated bases of continental thrust sheets or the sedimentary wedge [32]. On the other hand, Group III granites are post-collision calc-alkaline, derived from a mantle source thathasundergoneextensivecrustalcontaminationsimilartovolcanic-arcgranite.TheEğrigözgranitoidsare classified as volcanic-arc granite (VAG) and Group III granites (Figure 12a). Pearce *et al.* [33] proposed a tectonic classification of granitoids depending on Rb, Nb, and Y abundances in the Rb *versus* (Y + Nb) diagram. All data plotted in the VAG field are I-type due to their low contents of Rb, Nb and Y (Figure 12b). Because the ratios of the large ion lithophile (LIL) relative to high field strength (HFS) are increasing with increasing fractionation [34], the Eğrigöz granitoids are highly fractionated with an average LIL/HFS ratio of 6.6.

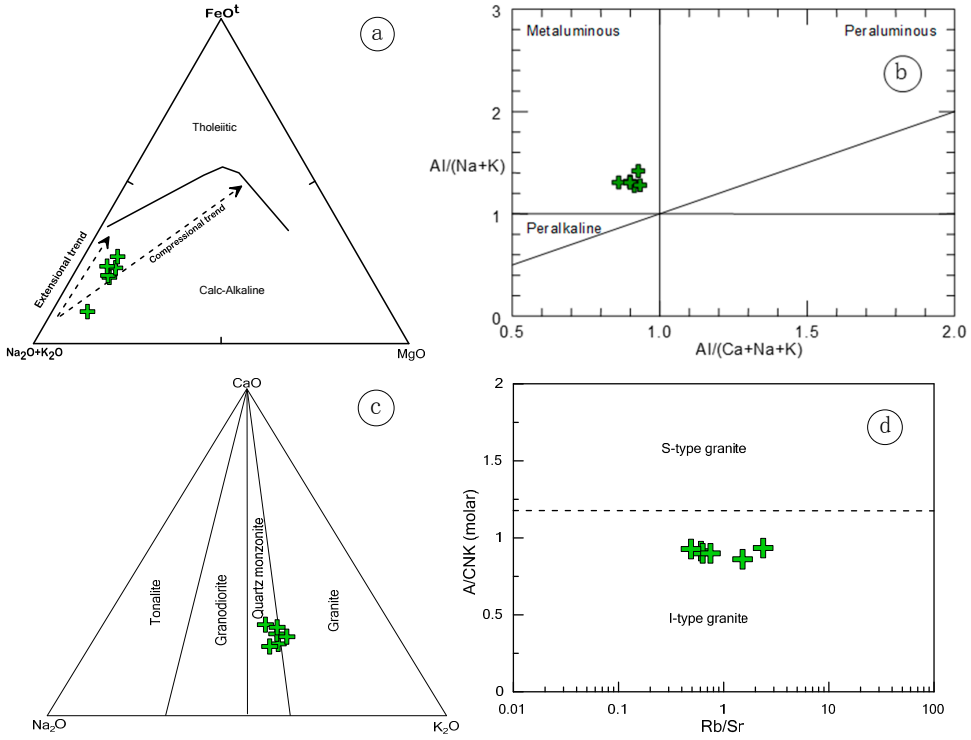


**Figure 11.** (**a**) AFM diagram for the studied granitic rocks, after [27], the compositional and extensional trend after [28]; (**b**) Molar A/NK *versus* A/CNK [29]; (**c**) $Na_2O$-CaO-$K_2O$ diagram for the studied granitoid rocks after [30]; (**d**) Molecular $Al_2O_3/(CaO + Na_2O + K_2O)$ *versus* Rb/Sr diagram showing the classification of the rocks into the fields of I-type and S-type granitoids [31].

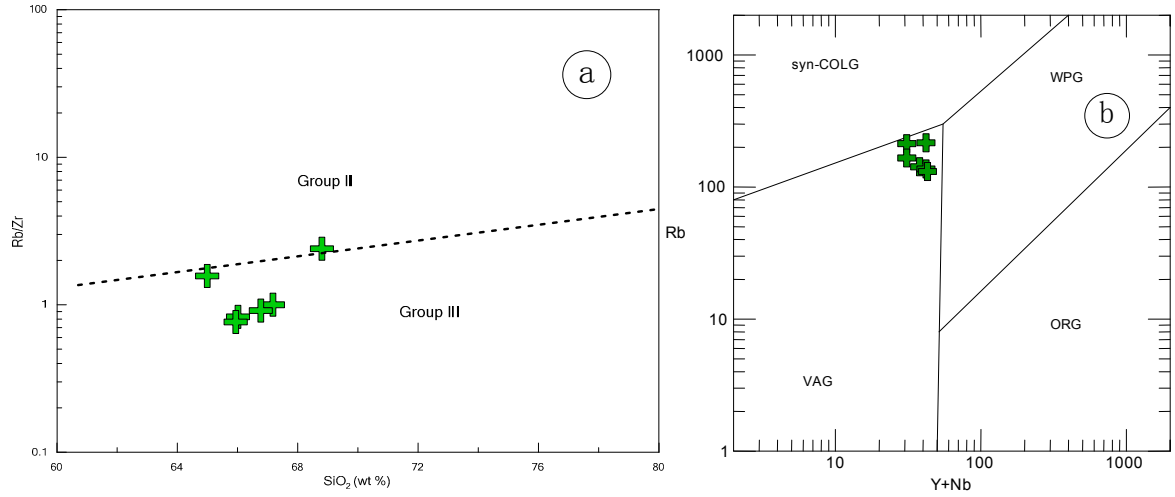


**Figure 12.** (**a**) Zr *versus* $SiO_2$ diagram for the studied Eğrigöz granitoids that indicating the Group III (post-collisional) affinity [32]; (**b**) Rb *versus* (Y + Nb) discrimination diagram [33]; syn-COLG: syn-collision granites; VAG: volcanic-arc granites; WPG: within-plate granites; ORG: ocean-ridge basalt.

#### 4.2.2. Alteration Geochemistry

The hydrothermally altered rocks in Eğrigöz granitoids include pervasive silicification, sulfidation, sericitization, and selective carbonatization and albitization which are distributed in three main alteration zones, based on the geological and petrographic studies. The major and trace elements of the altered rocks are shown in Table 2. The relative degree of alteration is determined by calculation of the chemical index of alteration (CIA = molar proportion $[Al_2O_3/(Al_2O_3 + CaO^* + Na_2O + K_2O)] \times 100)$) of Nesbitt and Young [35]. CIA ratios show that the altered rocks (an average of 58.1, 75.0, and 62.7 for zones 1, 2, and 3, respectively) were affected by a significant change in chemical composition with reference to the least-altered rocks (an average of 49.4). Generally, these hydrothermally altered rocks have higher iron content along with variable enrichments in $SiO_2$. They contain a large proportion of sulfide minerals (e.g., pyrite, chalcopyrite, sphalerite, galena and covellite) that display enrichments of Cu, Cu-Pb, and Cu-Pb-Zn in zones 1, 2, and 3, respectively. The wt % loss on ignition (LOI) increases significantly in samples displaying an intense alteration. An increase of $K_2O$ in zone 3 reflects sericitization/muscovite with chlorite and kaolinite, while zone 1 samples show local enrichment of CaO along with MgO and $Fe_2O_3$ relative to the least-altered rocks, which reflects the occurrence of carbonate alteration (calcite, ankerite and dolomite). The relationship between $Na_2O$ and $K_2O$ with the Ishikawa alteration index (Ishikawa AI = $[100(K_2O + MgO)/(K_2O + MgO + CaO + Na_2O)]$) of Ishikawa *et al.* [36] for the altered rocks shows that the data are plotted close to calcite/albite for zone 1, chlorite/sericite as well as dolomite/ankerite for zone 2, and chlorite/sericite for zone 3 (Figure 13a,b).

#### Mass-Balance Analyses

The mineralogical and bulk chemical changes reveal differences in the geochemical composition of the hydrothermally altered and unaltered rocks. Hydrothermal alteration associated with the brittle-ductile shear zones suggests the presence of a chemical ion exchange between the wall rocks and hydrothermal fluids, and its zonation reflects changes in the fluid composition with time and the interaction of this fluid with the host rocks [37]. The hydrothermal alteration processes are typically associated with the gain and loss of components of the entire rock mass [18].

Gresens [15] suggested that the composition-volume comparison of the altered and unaltered rocks is a useful way to determine changes in elemental compositions due to gains/losses or dilution. Grant [16,17] improved the equation of Gresens and suggested that the immobile elements should be plotted along an isocon line that has no mass transfer during the alteration processes. The recent version of software for determining and plotting mass balance/volume change during the alteration processes is the GEOISO-Windows™ program [21]. The mass balance/volume change by the absolute mobility of elements is determined by using Gresens' [15] equations and drawing the isocon diagrams of Grant [16]. This method requires selecting immobile elements to define a best-fit isocon line, which enables determination of mass gains/losses of the mobile elements in the altered rocks. The high field strength (HFS) elements, particularly Al, Ti, and Zr, were assumed to be immobile elements or their mobility was not significant during the alteration processes. In addition, in many studies, aluminum is considered immobile under low- to moderate-temperature hydrothermal and greenschist-grade metamorphic conditions [38]. When plotting $TiO_2$ *versus* $Al_2O_3$ in least-altered and altered rocks, a single trend of alteration is formed from the least-altered precursor to the altered samples (Figure 13c).

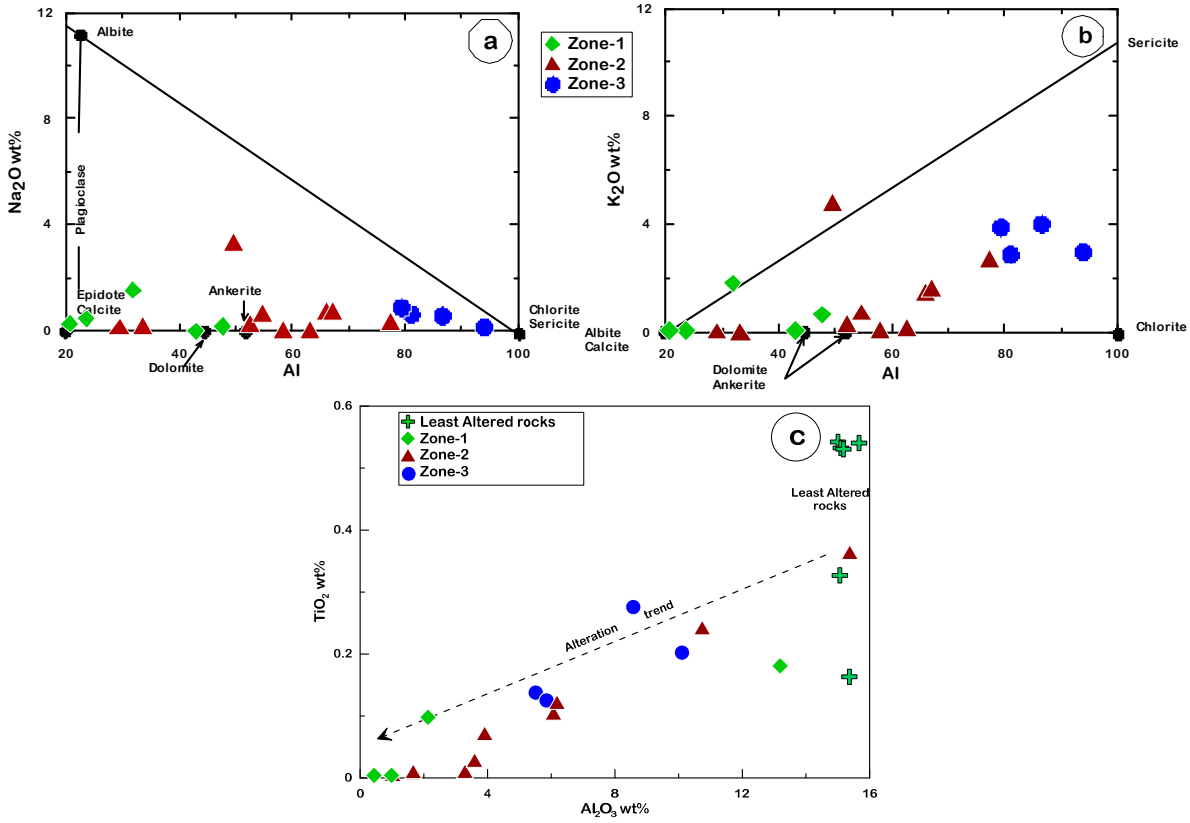


**Figure 13.** Relationship between alteration index (AI) and (**a**) $Na_2O$ and (**b**) $K_2O$ for the altered rocks [39]; (**c**) $TiO_2$-$Al_2O_3$ binary plot of the least-altered and altered rocks (alteration trend is the best fit line between the different samples).

The immobile elements in the three alteration zones were determined by drawing discrimination diagrams between the main immobile elements ($Al_2O_3$, $TiO_2$, and Zr) that are plotted around a slope of 1 (Figure 14). $Al_2O_3$ and $TiO_2$ are in zones 1 and 2 with an *R* (coefficient of determination value) of 0.79 and 0.92, respectively, whereas $Al_2O_3$ and Zr are the immobile elements in zone 3 with an *R* of 0.71.

Based on the mass and volume changes (gains and losses), each of the alteration zones has different additions and depletions of major/trace elements (Tables 3 and 4). According to mass balance calculations and isocon diagrams, samples from zone 1 have enrichment in $SiO_2$, $Fe_2O_3$, MgO, CaO, $Na_2O$, MnO, $SO_2$ and LOI with high S and Cu (Figures 15a and 16a,b). The mass change (MC) and volume change (VC) of this zone are calculated as 307.2 and 247.7, respectively. Samples from zone 2 exhibit enrichment of $SiO_2$, $Fe_2O_3$, MnO, $K_2O$, $SO_2$, and LOI with S, Cu, and Pb (Figures 15b and 16c,d), which led to estimated values of 183.6% MC and 156.0% VC. This zone has a lower amount of S and that refers to a local leaching and this leads to enrichment in Cu and Pb. Finally, common additions of $SiO_2$, $Fe_2O_3$, $K_2O$, $SO_2$, and LOI with significant S, Cu, Zn, and Pb enrichments characterize the major chemical changes in the altered rocks in zone 3 (Figures 15c and 16e,f) with 103.3% MC and 94.6% VC.

**Table 3.** Element/oxide mass changes in relation to original whole rock mass ((Mfi-Moi)/Mo) and in relation to original element/oxide mass in original rock ((Mfi-Moi)/Moi) (data from GEOISO-A Windows™ program).

| Sample ID | Zone 1 | | Zone 2 | | Zone 3 | |
|---|---|---|---|---|---|---|
| | (Mfi-Moi)/Mo | (Mfi-Moi)/Moi | (Mfi-Moi)/Mo | (Mfi-Moi)/Moi | (Mfi-Moi)/Mo | (Mfi-Moi)/Moi |
| $SiO_2$ | 174.8 | 2.6 | 131.6 | 2.0 | 81.0 | 1.2 |
| $Al_2O_3$ | 0.0 | 0.0 | 0.0 | 0.0 | 0.0 | 0.0 |
| $Fe_2O_3$ | 90.3 | 30.2 | 19.3 | 6.5 | 11.7 | 3.9 |
| MgO | 0.7 | 0.6 | −0.7 | −0.6 | −1.0 | −0.8 |
| CaO | 2.1 | 0.7 | −1.9 | −0.7 | −2.7 | −0.9 |
| $Na_2O$ | −1.5 | −0.4 | −1.7 | −0.5 | −2.5 | −0.7 |
| $K_2O$ | −3.2 | −0.6 | −1.8 | −0.3 | 1.6 | 0.3 |
| $TiO_2$ | −0.2 | −0.4 | −0.2 | −0.4 | −0.1 | −0.2 |
| $P_2O_5$ | −0.1 | −0.4 | −0.1 | −0.3 | −0.1 | −0.4 |
| MnO | 1.7 | 34.8 | 0.2 | 3.5 | 0.1 | 1.4 |
| $SO_2$ | 18.9 | 473.4 | 36.3 | 908.7 | 5.1 | 127.6 |
| LOI | 13.8 | 10.0 | 8.2 | 5.9 | 5.9 | 4.3 |
| As | 2737.7 | 131.6 | 1068.6 | 51.4 | 269.6 | 13.0 |
| Ba | 27.2 | 0.0 | −310.4 | -0.3 | 853.1 | 0.8 |
| Co | 180.4 | 9.0 | 128.0 | 6.4 | 40.6 | 2.0 |
| Cu | 50,265.7 | 3466.6 | 40,625.5 | 2801.8 | 30,310.9 | 2090.4 |
| Ga | 28.3 | 1.8 | 74.6 | 4.9 | −3.1 | −0.2 |
| Nb | 4.0 | 0.3 | 23.7 | 1.7 | −5.2 | −0.4 |
| Ni | 197.2 | 24.7 | 1487.8 | 18,597.1 | 18.4 | 2.3 |
| Pb | 5405.3 | 10,810.7 | 34,790.4 | 695.8 | 39,597.8 | 792.0 |
| Rb | −45.3 | −0.3 | −122.1 | −0.7 | 11.0 | 0.1 |
| S | 94,685.2 | 429.4 | 1819.4 | 825.1 | 25,563.1 | 115.9 |
| Sr | −67.6 | −0.3 | −131.7 | −0.7 | −81.6 | −0.4 |
| Y | 596.3 | 25.4 | 210.2 | 8.9 | 50.7 | 2.2 |
| Zn | 2192.3 | 5282.7 | 2234.7 | 5384.7 | 31,540.5 | 760.0 |
| Zr | 481.6 | 3.2 | 124.9 | 0.8 | 20.6 | 0.1 |

**Table 4.** Whole rock mass and volume change in different zones of alteration in the Tavşanlı area.

| Sample ID | Zone 1 | Zone 2 | Zone 3 |
|---|---|---|---|
| Whole rock mass change (MC) | 307.2 | 183.6 | 103.3 |
| Whole rock volume change (VC) | 247.8 | 156.0 | 94.7 |

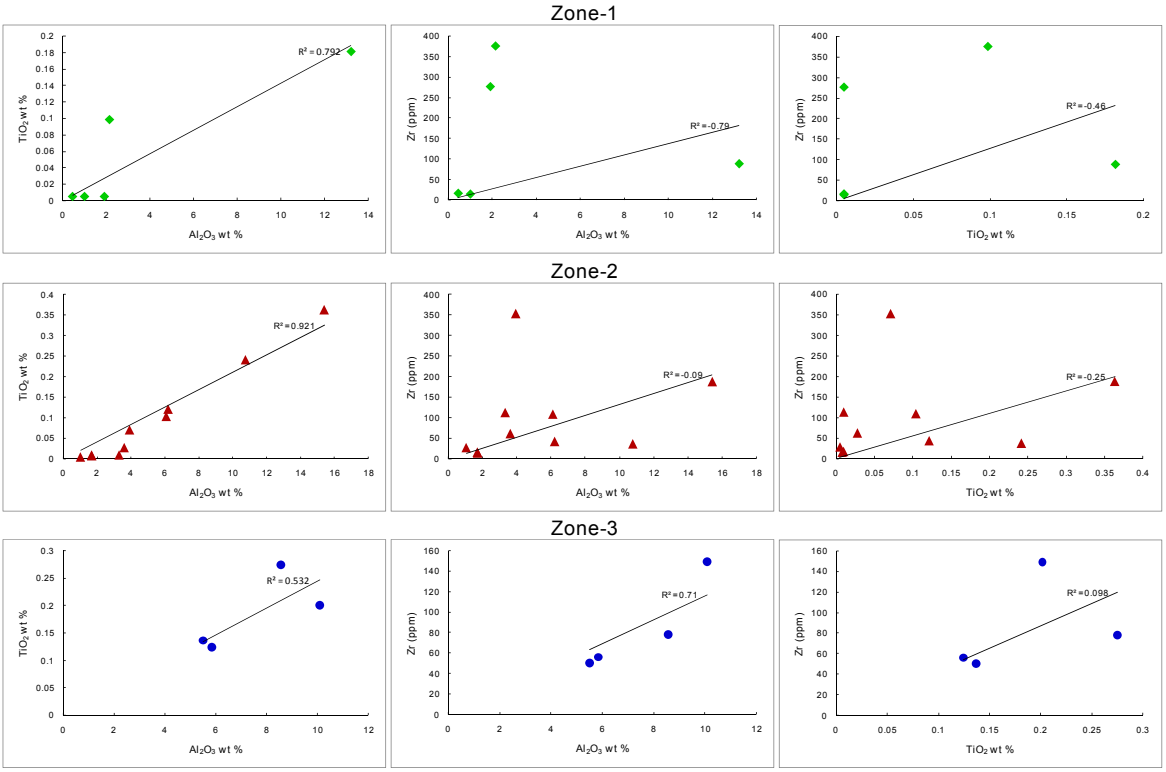


**Figure 14.** Immobile element discrimination diagrams of altered rocks of the Tavsanli area from zones 1, 2, and 3. Higher $R^2$ (coefficient of determination) value refers to a best fit indicating high immobility in a zone [40].

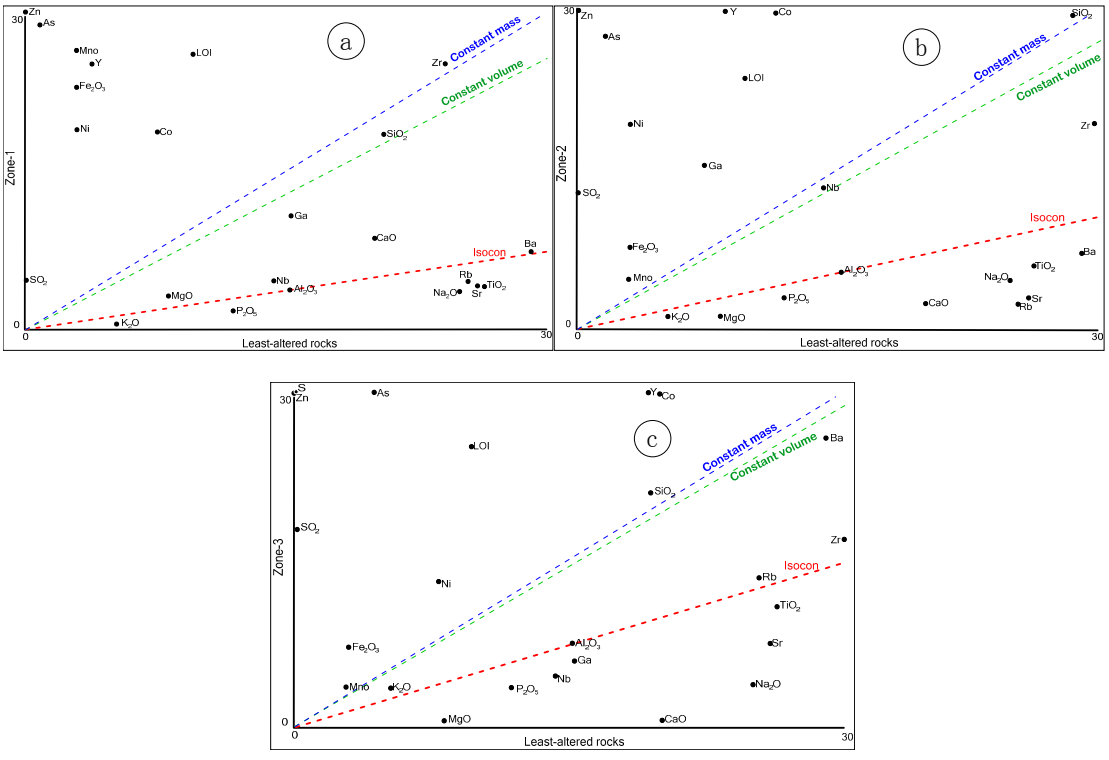


**Figure 15.** Isocon diagram comparing the mean composition of least-altered samples and altered samples from (**a**) zone 1, (**b**) zone 2, and (**c**) zone 3.

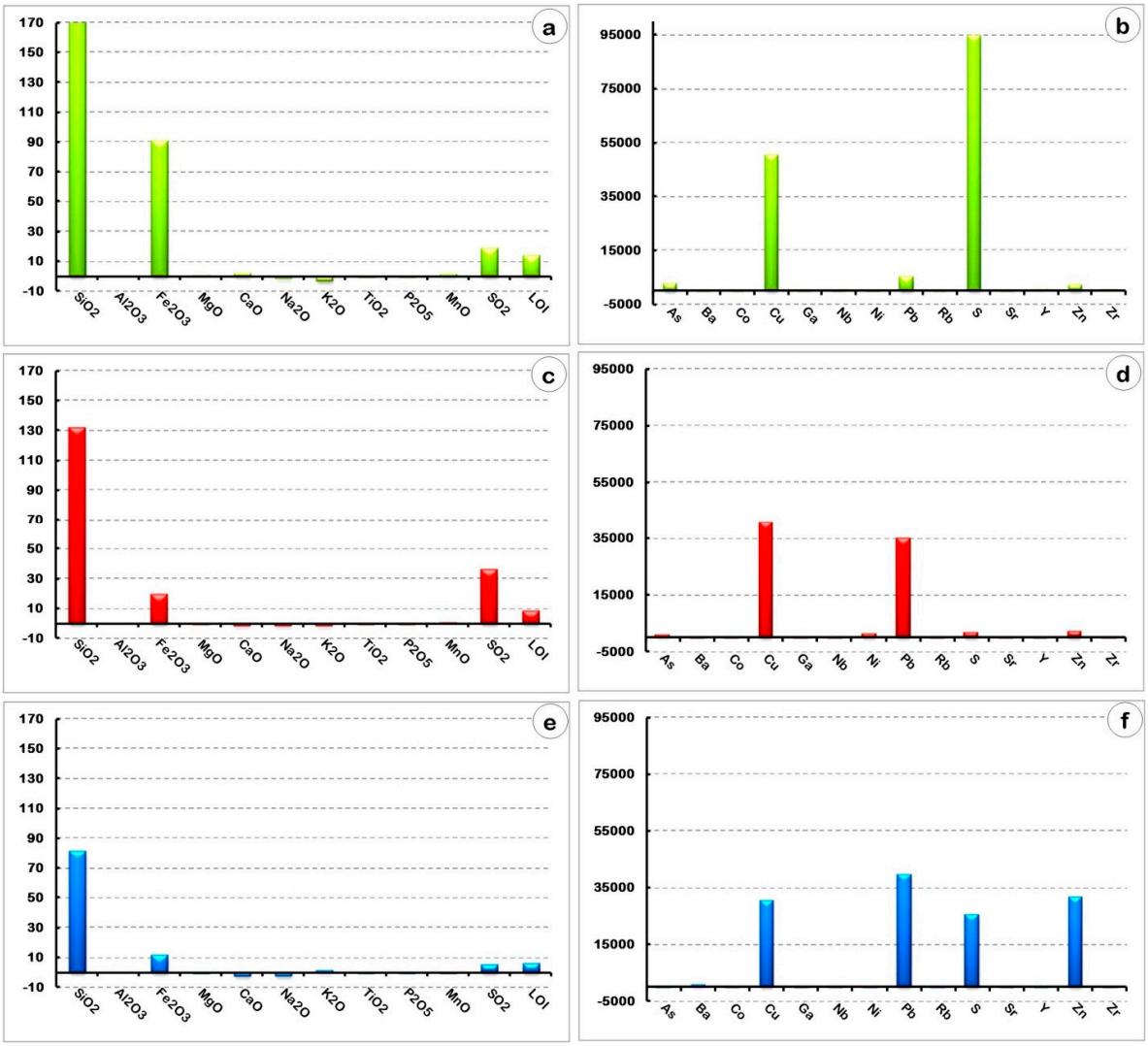


**Figure 16.** Profile-histograms showing the gain/loss of major oxides (wt %) and trace elements (ppm) during alteration in the different zones of hydrothermal alteration of the Tavşanlı area based on mean data of the least-altered samples as a reference for calculations, (**a**) and (**b**) for zone 1, (**c**) and (**d**) for zone 2, and (**e**) and (**f**) for zone 3.

## 5. Conclusions

In west Turkey, Mesozoic blueschist Tavsanli and greenschist Afyon terranes, which enclose the Balikesir-Kütahya (or Bursa-Kütahya) district, are dominated by early Miocene plutonic-hosted, volcanic-hosted, and low-sulfidation epithermal Au deposits. This district was controlled by NE- to ENE-trending graben systems, including early Miocene (20–18 Ma) syn-tectonic Eğrigöz granitoid intrusions [41]. The Cu, Pb-Zn, W or Mo skarn that are distributed throughout Turkey are closely associated with porphyry systems in this district [41]. This mineralization is confined to NW-trending faults that are commonly associated with pervasive hydrothermal alterations, brecciation, and quartz stockwork veinlets.

Three main alteration zones with gradual boundaries border the mineralized quartz veins and/or shear zone in the mine area; zone 1 (silicified/iron carbonatized alterations ± albite), zone 2 (argillic-silicic alterations), and zone 3 (phyllic alterations). Zone 1 occurs in the center and has high amounts of chalcopyrite and pyrite. Zone 2 occurs along with zone 1 in the north, characterized by high amounts of chalcopyrite, sphalerite and pyrite. Zone 3 is in southern contact with zone 1 with

high amounts of chalcopyrite, sphalerite and galena with pyrite. The ore minerals, *i.e.*, chalcopyrite, sphalerite, galena, covellite, malachite, azurite and pyrite, are abundant at the contact between quartz veins and the altered rocks as well as in disseminations in the alteration zones. A three-fold paragenetic sequence was likely responsible for the ore deposition, including the pre-ore, hydrothermal ore, and supergene stages.

The Eğrigöz monzogranitic and quartz monzonitic rocks represent the least-altered rocks. These rocks are metaluminous and calc-alkaline rocks classified as I-type VAG granite. Representative samples from the different alteration zones have high CIA relative to the least-altered rocks. The high Fe contents are probably caused by sulphidation with chloritization along with silicification. Based on the values of the changes (gain and loss) of mass and volume, each alteration zone has different major/trace additions and depletions calculated by the GEOISO-Windows™ program assuming Al, Ti, and Zr are immobile elements or their mobility was not significant during the alteration processes. Samples from zone 1 have enrichment in $SiO_2$, $Fe_2O_3$, MgO, CaO, $Na_2O$, MnO, $SO_2$, and LOI with high S and Cu. Zone 2 has rocks enriched in $SiO_2$, $Fe_2O_3$, MnO, $K_2O$, $SO_2$, and LOI with S, Cu, and Pb. Zone 3 samples have enrichment of $SiO_2$, $Fe_2O_3$, $K_2O$, $SO_2$, and LOI with significant amounts of S, Cu, Zn, and Pb. Based on these data, the zonal arrangement of zones 1, 2, and 3 gives the impression of non-systematic distribution of alterations around the ore vein in the center from silicic-carbonate alterations +/− albitization to phyllic-argillic alterations with increased base metals (Cu-Pb-Zn) from Cu, Cu-Pb, to Cu-Pb-Zn in zones 1, 2, and 3, respectively. Therefore, the studied Cu-Pb-Zn mineralization is mainly linked with the quartz veins within the main silicic and carbonate alteration types along the NW fault system which post-dated the Eğrigöz intrusion. Furthermore, the morphology of these quartz veins and superimposed alteration types imply a significant role of shearing in the mobilization of metals and ore deposition from the host intrusion.

**Acknowledgments:** This study was financially supported by the BAP Project (No. 37860) by Istanbul Technical University (ITU), Turkey. The authors are grateful to Paul A. Schroeder (University of Georgia, USA) and Fuat Yavuz (ITU, Turkey) for critical reading, providing language help, and improving an earlier version of this manuscript, as well as to Muhittin Karaman (ITU, Turkey). Additionally, the authors are much more grateful to the editor and the anonymous reviewers for their constructive comments, corrections and helpful suggestions which greatly improved the manuscript.

**Author Contributions:** Mustafa Kumral did the field work together with Amr Abdelnasser, as well as the ore geology part. Amr Abdelnasser contributed the classification and geochemistry of hydrothermal alteration zones around the mineralized veins, with Mustafa Kumral. Murat Budakoglu completed the geochemical characteristics of the least-altered host rocks. All authors participated in the writing of the earlier and last versions of this manuscript.

**Conflicts of Interest:** The authors declare no conflict of interest.

## References

1. Janković, S. The Carpatho-Balkanides and adjacent area: A sector of the Tethyan Eurasian metallogenetic belt. *Miner. Depos.* **1997**, *32*, 426–433.
2. Kuşcu, İ.; Kuşcu, G.G.; Tosdal, R.M.; Ulrich, T.D.; Friedman, R. Magmatism in the southeastern Anatolian orogenic belt: Transition from arc to post-collisional setting in an evolving orogen. *Geol. Soc. Lond. Spec. Publ.* **2010**, *340*, 437–460. [CrossRef]
3. Borsi, S.; Ferrara, G.; Innocenti, F.; Mazzuoli, R. Geochronology and petrology of recent volcanics in the Eastern Aegean Sea. *Bull. Volcanol.* **1972**, *36*, 473–496. [CrossRef]
4. Fytikas, M.; Giuliani, O.; Innocenti, F.; Marinelli, G.; Mazzuoli, A. Geochronological data on recent magmatism of the Aegean Sea. *Tectonophysics* **1976**, *31*, 29–34. [CrossRef]
5. Delaloye, M.; Bingol, E. Granitoids from western and northwestern Anatolia: Geochemistry and modeling of geodynamic evolution. *Int. Geol. Rev.* **2000**, *42*, 241–268. [CrossRef]
6. Altunkaynak, Ş.; Dilek, Y.; Genç, C.Ş.; Sunal, G.; Gertisser, R.; Furnes, H.; Foland, K.A.; Yang, J. Spatial, temporal and geochemical evolution of Oligo-Miocene granitoid magmatism in western Anatolia, Turkey. *Gondwana Res.* **2012**, *21*, 961–986. [CrossRef]

7. Okay, A.I. Metamorphic belts in northwest Anatolia. In *Ketin Symposium*; Geological Society of Turkey: Ankara, Turkey, 1985; pp. 83–92. (In Turkish)
8. Hasözbek, A.; Akay, E.; Erdoğan, B.; Satır, M.; Siebel, W. Early Miocene granite formation by detachment tectonics or not? A case study from the northern Menderes Massif (Western Turkey). *J. Geodyn.* **2010**, *50*, 67–80. [CrossRef]
9. Özgenç, İ.; İlbeyli, N. Petrogenesis of the Late Cenozoic Eğrigöz Pluton in Western Anatolia, Turkey: Implications for magma genesis and crustal processes. *Int. Geol. Rev.* **2008**, *50*, 375–391. [CrossRef]
10. Oyman, T.; Özgenç, İ.; Tokcaer, M.; Akbulut, M. Petrology, geochemistry, and evolution of the iron skarns along the northern contact of the Eğrigöz Plutonic Complex, Western Anatolia, Turkey. *Turk. J. Earth Sci.* **2013**, *22*, 61–97.
11. Uğurcan, O.G.; Oyman, T. Mineralogy, Mineral Chemistry and Fluid Inclusion data From Kalkan and Karaağıl (Simav-Kütahya) Iron Skarns. In Proceedings of the 8th International Symposium on Eastern Mediterranean Geology (ISEMG), Muğla, Turkey, 13–17 October 2014.
12. Göncüoğlu, M.C.; Dirik, K.; Kozlu, H. Pre-alpine and alpine terranes in Turkey: Explanatory notes to the terrane map of Turkey. *Ann. Geol. Pays Hell.* **1996**, *37*, 515–536.
13. Konak, N. *Geological Map of Turkey in 1/500.000 Scale: İzmir Sheet*; Mineral Research and Exploration Directorate of Turkey (MTA): Ankara, Turkey, 2002.
14. Ring, U.; Collins, A.S. U-Pb SIMS dating of synkinematic granites; timing of core-complex formation in the northern Anatolide Belt of western Turkey. *Geol. Soc. Lond.* **2005**, *162*, 289–298. [CrossRef]
15. Gresens, R.L. Composition-volume relationships of metasomatism. *Chem. Geol.* **1967**, *2*, 47–65. [CrossRef]
16. Grant, J.A. The isocon diagram; a simple solution to Gresens' equation for metasomatic alteration. *Econ. Geol.* **1986**, *81*, 1976–1982. [CrossRef]
17. Grant, J.A. Isocon analysis: A brief review of the method and applications. *Phys. Chem. Earth* **2005**, *30*, 997–1004. [CrossRef]
18. Middelburg, J.J.; van der Weijden, C.H.; Woittiez, J.R.W. Chemical processes affecting the mobility of major, minor and trace elements during weathering of granitic rocks. *Chem. Geol.* **1988**, *68*, 253–273. [CrossRef]
19. Leitch, C.H.B.; Lentz, D.R. The Gresens approach to mass balance constraints of alteration systems: Methods, pitfalls, examples. *Alter. Alter. Process. Assoc. Ore-Form. Syst. Geol. Assoc. Can. Short Course Notes* **1994**, *11*, 161–192.
20. Carr, M. *Igpet 2007 for Windows XP or Vista*; Terra Softa Inc: Somerset, NJ, USA, 2007.
21. Coelho, J. GEOISO—A Windows™ program to calculate and plot mass balances and volume changes occurring in a wide variety of geologic processes. *Comput. Geosci.* **2006**, *32*, 1523–1528. [CrossRef]
22. Akdeniz, N.; Konak, N. Simav–Emet–Dursunbey–Demirci yörelerinin jeolojisi (Geology of the Simav–Emet–Dursunbey–Demirci areas). In *Bulletin of Mineral Research and Exploration Institute of Turkey (Unpublished) Report*; MTA: Ankara, Turkey, 1979; p. 6547. (In Turkish)
23. Işık, V.; Tekeli, O. Late orogenic crustal extension in the Northern Menderes Massif (western Turkey): Evidences for metamorphic core complex formation. *Int. J. Earth Sci.* **2001**, *89*, 757–765.
24. Okay, A.I.; Satır, M.; Maluski, H.; Siyako, M.; Monie, P.; Metzger, R.; Akyüz, S. Paleo-and Neo-Tethyan events in northwestern Turkey: Geologic and geochronologic constraints. *World Reg. Geol.* **1996**, *1*, 420–441.
25. Streckeisen, A. To each plutonic rock its proper name. *Earth Sci. Rev.* **1976**, *12*, 1–33. [CrossRef]
26. Sibson, R.H. Controls on maximum fluid overpressure defining conditions for mesozonal mineralization. *J. Struct. Geol.* **2004**, *26*, 1127–1136. [CrossRef]
27. Irvine, T.N.; Baragar, W.R.A. A guide to chemical classification of the common volcanic rocks. *Can. J. Earth Sci.* **1971**, *8*, 523–548. [CrossRef]
28. Petro, W.L.; Vogel, T.A.; Wilband, J.T. Major-element chemistry of plutonic rock suites from compressional and extensional plate boundaries. *Chem. Geol.* **1979**, *26*, 217–235. [CrossRef]
29. Maniar, P.D.; Piccoli, P.M. Tectonic discrimination of granitoids. *Geol. Soc. Am. Bull.* **1989**, *101*, 635–643. [CrossRef]
30. Hunter, D.R.; Barker, F.; Millard, H.T. The geochemical nature of the Archean ancient gneiss complex and granodiorite suite, Swaizland: A preliminary study. *Precambrian Res.* **1978**, *7*, 105–127. [CrossRef]
31. Chappell, B.W.; White, A.J.R. Two contrasting granite types. *Pac. Geol.* **1974**, *8*, 173–174.
32. Harris, N.B.W.; Pearce, J.A.; Tindle, A.G. Geochemical Characteristics of Collision-Zone Magmatism. *Geol. Soc. Lond. Spec. Publ.* **1986**, *19*, 67–81. [CrossRef]

33. Pearce, J.A.; Lippard, S.J.; Roberts, S. Characteristics and tectonic significance of supra-subduction zone ophiolites. *Geol. Soc. Lond. Spec. Publ.* **1984**, *16*, 77–94. [CrossRef]
34. Saunders, A.D.; Tarney, J.; Weaver, S.D. Transverse geochemical variations across the Antarctic Peninsula: Implications for the genesis of calc-alkaline magmas. *Earth Planet. Sci. Lett.* **1980**, *46*, 344–360. [CrossRef]
35. Nesbitt, H.W.; Young, G.M. Early Proterozoic climates and plate motions inferred from major element chemistry of lutites. *Nature* **1982**, *199*, 715–717. [CrossRef]
36. Ishikawa, Y.; Sawaguchi, T.; Iwaya, S.; Horiuchi, M. Delineation of prospecting targets for Kuroko deposits based on modes of volcanism of underlying dacite and alteration halos. *Min. Geol.* **1976**, *26*, 105–117.
37. Meyer, C.; Hemley, J.J. Wall rock alteration. *Geochem. Hydrotherm. Ore Depos.* **1967**, *1*, 166.
38. Barton, M.D.; Ilchik, R.P.; Marikos, M.A. Metasomatism. *Rev. Mineral. Geochem.* **1991**, *26*, 321–349.
39. Large, R.R.; Gemmell, J.B.; Paulick, H.; Huston, D.L. The alteration box plot: A simple approach to understanding the relationship between alteration mineralogy and lithogeochemistry associated with VHMS deposits. *Econ. Geol.* **2001**, *96*, 957–972.
40. Wartman, J.M. Physical Volcanology and Hydrothermal Alteration of the Rainy River Gold Project, Northwest Ontario. Ph.D. Thesis, University of Minnesota, Minneapolis, MN, USA, 2011.
41. Rabayrol, F.; Mišković, A.; Hart, C.J.R.; Kuşcu, I.; Sanchez, M. The Cenozoic metallogeny of Western Anatolia, Turkey. In Proceedings of the SEG 2014 Conference, Denver, CO, USA, 26–31 October 2014.